Title: Obesity promotes urinary tract infection by disrupting urothelial immune defenses

Authors: Laura Schwartz[1,2], Kristin Salamon[1], Aaron Simoni[1], Israel Cotzomi-Ortega[1], Yuriko Sanchez-Zamora[1], Sarah Linn-Peirano[1,3], Preeti John[1], Juan de Dios Ruiz-Rosado[1,2], Ashley R. Jackson[1,2], Xin Wang[1], and John David Spencer[1,2,*]

Affiliations:
[1]The Kidney and Urinary Tract Center, The Abigail Wexner Research Institute at Nationwide Children's, Columbus, OH USA

[2]Division of Nephrology and Hypertension, Department of Pediatrics, The Ohio State University College of Medicine and Nationwide Children's, Columbus, OH USA

[3]College of Veterinary Medicine, University of Tennessee Institute of Agriculture, Knoxville, TN, USA

***Correspondence to**:
John David Spencer
700 Children's Dr, WA4016
Columbus, OH 43205
Email: John.Spencer@nationwidechildrens.org

Author Contributions: L.S. and J.D.S. supervised the project and contributed to the design and interpretation of all experiments. K.S. managed the mouse colony and completed the *in vivo* mouse experiments. K.S., A.S., P.J., and J.R-R. performed mouse biometric testing, flow cytometry, or Western blotting. X.W. and L.S. analyzed the limiting cell RNA-seq. L.S., S.L.P., and A.R.J. completed immunostaining and microscopy. L.S., I.C-O., and Y.S-Z. performed the *ex vivo* and *in vitro* experiments. L.S. and J.D.S. wrote the manuscript with input from all authors.

Competing Interest Statement: The authors declared that no conflict of interest exists.

This PDF file includes:

Main Text
Figures 1 to 6

ABSTRACT:

Obesity is a significant public health concern that is associated with numerous health risks. Infections are a major complication of obesity, but the mechanisms responsible for increased infection risk are poorly defined. Here, we use a diet induced obesity mouse model and investigate how obesity impacts urinary tract infection (UTI) susceptibility and bladder immune defenses. Our results show that high-fat diet fed female and male mice exhibit increased susceptibility to uropathogenic *E. coli* (UPEC) following experimental UTI. Transcriptomic analysis of bladder urothelial cells shows that obesity alters gene expression in a sex-specific manner, with distinct differentially expressed genes in male and female mice, but shared activation of focal adhesion and extracellular matrix signaling. Western blot and immunostaining confirm activation of focal adhesion kinase, a central component of the focal adhesion pathway, in the bladders of obese female and male mice. Mechanistically, experiments using primary human urothelial cells demonstrate that focal adhesion kinase overexpression promotes UPEC invasion. These findings demonstrate that obesity enhances UTI susceptibility by activating focal adhesion kinase and promoting bacterial invasion of the urothelium. Together, they explain how obesity promotes UTI vulnerability and identify modifiable targets for managing obesity-associated UTI.

INTRODUCTION:

Obesity is a major public health challenge affecting over a billion people globally (1). Obesity can lead to chronic health issues, including type 2 diabetes, cardiovascular disease, nonalcoholic fatty liver disease, neurodegenerative disorders, and increased cancer risk. Beyond its direct health effects, obesity places a significant burden on healthcare systems, reduces overall productivity, quality of life, and life expectancy (2, 3).

Infections are a significant yet overlooked consequence of obesity. Obesity increases susceptibility to nosocomial, surgical site, and community-acquired infections (4, 5). Among the common community-acquired infections, obesity has been identified as an independent risk factor for urinary tract infections (UTI) in both males and females across the lifespan (4-11). Obese individuals with UTI are 2.5 times as likely to require hospitalization compared to their non-obese counterparts (12, 13). Among hospitalized patients, those with obesity are more likely to develop UTI, which can prolong hospital stays (4, 14-16). Obese individuals are nearly five times more likely to develop pyelonephritis, with young girls and women at highest risk (6, 17). Additionally, in kidney transplant recipients, for whom UTI is a significant risk factor for allograft loss, obesity is a significant risk factor for UTI, with obese patients at 4.7 times higher UTI risk than non-obese patients (18). Beyond acute and severe UTIs, obesity is associated with recurrent infections, underscoring its broader impact on urinary tract health (7). Together, these clinical outcomes reveal a critical gap in our understanding of how obesity influences UTI pathogenesis and highlight the need to define mechanisms driving increased infection risk in order to improve UTI prevention and treatment strategies.

Uropathogenic *Escherichia coli* (UPEC) is the leading cause of UTIs (19). The bladder employs a multifaceted defense system to prevent UPEC infection. In the bladder, the urothelium serves as a critical physical barrier that resists UPEC invasion, reinforced by tightly joined umbrella cells, a uroplakin- and glycosaminoglycan-coated surface, and tight junctions (20). Additionally, the

urothelium secretes antimicrobial peptides that directly kill bacteria. Upon pathogen detection, the urothelium activates pattern recognition receptors, triggering downstream transcription factors that promote the expression of antimicrobial peptides as well as cytokines or chemokines. These immune mediators recruit myeloid cells to clear UPEC (20-23).

Despite this integrated urothelial defense network to prevent UTI, UPEC have evolved mechanisms to invade and persist within the bladder. Using adhesive organelles called type 1 pili, UPEC bind to host receptors and are internalized by urothelial cells. Once inside, UPEC can evade host immune responses and resist antibiotics. Intracellular UPEC niches may contribute to UTI severity, particularly when urothelial defenses are impaired (23, 24). However, how obesity influences UTI pathogenesis and bladder defenses remains poorly understood.

This study investigates how obesity affects urothelial antibacterial defenses and impacts UTI risk. We utilize a diet induced obesity mouse model that mirrors human obesity in several ways – including weight gain, insulin resistance, and altered lipid metabolism (25, 26). Mice are fed a high-fat diet (HFD), consisting of 45-60% of calories from fat, to induce obesity. The metabolic abnormalities observed in HFD-fed mice closely parallel human obesity progression, with early weight gain by 2-4 weeks and marked metabolic dysfunction by 12-16 weeks (25, 26). Because male mice develop more severe obesity and metabolic impairment than females, we also assess sex-specific differences in obesity-associated immune and urothelial responses (25-28). To enhance translational relevance, our preclinical findings are validated in primary human urothelial cultures. Using these complementary models, we show that obesity increases UPEC susceptibility via activation of focal adhesion kinase (FAK) signaling in male and female mice. FAK overexpression promotes UPEC invasion, revealing a mechanistic pathway through which obesity augments UTI vulnerability.

RESULTS:

Obesity increases UTI susceptibility in female mice. To determine whether obesity impacts UPEC vulnerability, female mice were fed either standard chow (SC) or a HFD for 4, 8, or 12 weeks. These timepoints allow us to study the early (4 weeks), progressive (8 weeks), and sustained effects of obesity (12 weeks). After 4 weeks, HFD-fed mice exhibited an 18% increase in body weight compared to SC mice, along with mild elevations in blood glucose concentrations and impaired glucose disposal observed with glucose tolerance testing. These metabolic disturbances became more pronounced at 8 and 12 weeks. By 12 weeks, HFD-fed mice gained 44% more body weight compared to SC-fed mice and developed more pronounced insulin resistance, as assessed by glucose tolerance testing (**Figure 1A-C**). Female mice did not meet criteria for diabetes, defined by non-fasting blood glucose concentrations ≥ 250 mg/dL or the presence of glucosuria (29). To assess systemic inflammation, we measured serum concentrations of proinflammatory cytokines, but detected no significant differences between SC- and HFD-fed mice (**Supplemental Table 1**).

Given these metabolic impairments, we next assessed whether obesity influences UTI susceptibility. Twenty-four hours after transurethral UPEC infection, HFD-fed mice exhibited greater urine and bladder UPEC titers compared to SC mice (**Figure 1D**). Notably, UPEC burden differences increased with the duration of HFD exposure. Compared to SC fed mice, mice receiving a HFD for 4 weeks had a 2.4-fold increase in mean bladder UPEC CFUs. After 8 and 12 weeks, mean bladder CFUs increased 6.4-fold 24 hours after infection. To determine whether UPEC infection persisted, we enumerated urine and bladder UPEC colonies 48 hours post-infection in mice maintained on HFD or SC for 8 weeks. HFD-fed mice had sustained elevations in UPEC titers compared to SC-fed controls (**Figure 1D**).

Obesity also increases UPEC vulnerability in male mice. Because sex affects diet-induced obesity outcomes, we next evaluated UTI susceptibility in male mice fed either a HFD or SC. By 8 weeks on a HFD, male mice gained 24% more weight compared to SC-fed mice, and by 12 weeks, HFD-fed mice gained 48% more weight compared to SC controls (**Figure 2A**). Compared to female mice, metabolic impairments were more pronounced in males, with significant elevations in blood glucose concentrations and impaired glucose disposal on glucose tolerance testing, particularly after 12 weeks on a HFD (**Figure 2B/C**). Like female mice, HFD-fed male mice did not develop glucosuria and had comparable serum cytokine concentrations (**Supplemental Table 1**). Following direct bladder UPEC infection, HFD-fed male mice had greater urine and bladder UPEC titers at both 24- and 48-hours post-infection (**Figure 2D**). By 8 and 12 weeks, mean bladder UPEC CFUs were 2.5-fold higher in HFD-fed male mice compared to SC-fed mice 24 hours after infection, while mean urine burden increased 2-fold and 970-fold, respectively. These findings demonstrate that obesity enhances UTI susceptibility in both male and female mice.

Obesity augments UTI susceptibility independent of changes in immune cell recruitment and antibacterial function. Myeloid cells, including macrophages and neutrophils, have essential roles in UPEC clearance by migrating to the site of infection, phagocytosing bacteria, and killing pathogens (22, 23). To determine whether diet-induced obesity impairs their recruitment or function, we used flow cytometry to quantify myeloid populations in UPEC infected bladders from male and female mice fed a HFD or SC for 8 or 12 weeks. Recruitment of neutrophils, monocytes, and both M1-like and M2-like macrophages was comparable between HFD-fed and SC mice. Although differences in infection technique prevent direct sex comparisons, we observed fewer neutrophils, monocytes, and macrophages in male mice (SC and HFD) at 8 weeks compared to female mice. Similar trends were observed for monocytes and

M2-like macrophages in the 12-week cohort – consistent with prior data showing greater immune cell infiltration in infected female bladders (**Supplemental Figure 1**).(30)

To assess immune cell function, we evaluated myeloid cell phagocytosis, intracellular UPEC killing, and *ex vivo* bacterial killing by neutrophils from SC and HFD-fed mice. We observed comparable UPEC uptake as well as intracellular and extracellular killing between diet groups (**Supplemental Figures 2 and 3**). Phagocytic activity was reduced in male neutrophils, monocytes, and macrophages (**Supplemental Figure 2**) – supporting published data that phagocytic capacity may be impacted by sex (30). Together, these findings suggest that the increased bacterial burden observed in HFD-fed mice is not due to defects in immune cell infiltration or antibacterial function.

Obesity alters gene expression in the bladder urothelium. Since obesity did not impair myeloid cell recruitment or bacterial killing, we examined whether obesity impacts urothelial defenses. We performed limiting cell RNA-seq on non-infected bladder urothelium from female and male mice fed SC or a HFD for 12 weeks (*n*=4/cohort, **Figure 3**, **Supplemental Dataset 1**). To validate these findings, an additional RNA-seq analysis was performed in a smaller number of non-infected female and male mice maintained on SC or a HFD for 8 weeks (*n*=3/cohort, **Supplemental Figure 4**, **Supplemental Dataset 2**). Principal component analysis (PCA) demonstrated that urothelial gene expression profiles were consistent among mice within the same diet group but differed between HFD-fed and SC mice, with the greatest variance captured along principal component 1 (**Figure 3A/D and Supplemental Figure 4**). Heatmaps of the differentially expressed genes (DEGs, false discovery rate < 0.05) demonstrated distinct diet-dependent gene expression patterns in both sexes (**Figure 3B/E and Supplemental Figure 4**). These findings indicate that a HFD induces transcriptional changes in the urothelium, suggesting a urothelial-intrinsic response to metabolic stress.

In urothelium from 12-week HFD-fed female mice, 173 genes were up-regulated and 25 genes were down-regulated compared to SC mice (**Figure 3C**). In urothelium from 12-week HFD-fed male mice, 125 genes were up-regulated and 51 genes were down-regulated compared to SC mice (**Figure 3F**). At 8 weeks, urothelium from HFD-fed female mice had 1,812 up-regulated and 1,064 down-regulated genes, whereas HFD-fed male mice had 94 up-regulated and 215 suppressed genes (**Supplemental Figure 4**). The reason for the higher number of DEGs in females after 8 weeks of HFD compared to the 12-week cohort is unclear. While smaller sample sizes often reduce statistical power and result in fewer DEGs, it is possible that this early response may reflect acute transcriptional remodeling or underlying metabolic variability.

Diet-induced obesity alters urothelial gene expression in a sex-specific manner. Transcriptomic analysis revealed that obesity differentially affects gene expression in female and male urothelium, with minimal overlap in DEGs between sexes. At 12 weeks on a HFD, only two genes were commonly up-regulated in both male and female urothelium, and no genes were commonly down-regulated (**Figure 4A**). A similar pattern was observed at 8 weeks, with just 2 shared up-regulated and 3 shared down-regulated genes (**Supplemental Figure 5**). Despite this minimal gene-level overlap, pathway enrichment analysis showed convergence in the biological processes affected by obesity. Kyoto Encyclopedia of Genes and Genomes (KEGG) pathway enrichment analysis demonstrated that up-regulated genes in HFD mice of both sexes were enriched for pathways related to focal adhesion, extracellular matrix (ECM)-receptor interaction, and cytoskeleton organization (**Figure 4B and Supplemental Figure 5**). Down-regulated genes at 8 and 12 weeks on the diet enriched KEGG pathways related to cancer, however the biological significance of this is unclear due to low enrichment scores and a small number of contributing genes (**Figure 4B and Supplemental Figure 5**). Thus, while obesity drives largely sex-specific

changes at the individual gene level, it also induces common transcriptional shifts in pathways involved in cellular architecture and tissue remodeling.

To investigate how obesity affects established urothelial defenses against UPEC, we profiled the expression of genes involved in innate immunity and epithelial barrier integrity (22, 23). While 12 weeks of HFD had limited impact on innate immune gene expression, genes associated with bladder barrier function and uroplakin plaque formation were disrupted in a sex-specific manner (**Figure 4C**). In females, most bladder barrier genes were suppressed, while in males, many of the same genes were up-regulated. Additionally, genes associated with the KEGG-enriched pathways identified above – including focal adhesion, ECM-receptor interaction, and cytoskeletal organization – were broadly up-regulated in both sexes, with more pronounced changes in HFD-fed female mice (**Figure 4C**). Similar trends were observed at 8 weeks of HFD feeding (**Supplemental Figure 5**). These results suggest that obesity remodels the urothelium, impacting both the apical surface and the cell-ECM interface, potentially compromising the urothelial barrier and increasing susceptibility to UTI.

Diet-induced obesity activates focal adhesion kinase. Since our transcriptomic analysis revealed enrichment and activation of focal adhesion, ECM-receptor interaction, and cytoskeletal signaling pathways in the urothelium of HFD-fed female and male mice, we next investigated whether obesity alters the urothelial-ECM interface. Focal adhesion kinase (FAK), a non-receptor tyrosine kinase, serves as a central hub for these pathways, integrating signals from the ECM and coordinating downstream intracellular responses, including cytoskeletal remodeling (31, 32). Based on this role, we hypothesized that FAK mediates obesity-driven changes in urothelial structure that promote UPEC infection.

FAK is regulated post-translationally. Upon binding to integrins, it undergoes autophosphorylation and recruits downstream effectors such as PI3K/AKT (31, 32). In urothelium from 12-week HFD-

fed female and male mice, Western blot revealed increased FAK and AKT phosphorylation compared to SC controls (**Figure 5A/C).** FAK activation was also observed at 8 weeks of HFD feeding **(Supplemental Figure 6**). Immunostaining confirmed increased FAK expression in the bladder urothelium of mice at both 8 and 12 weeks (**Figure 5B/D and Supplemental Figure 7**). These results corroborate our transcriptomic findings and demonstrate that obesity activates urothelial FAK signaling, which may increase UPEC susceptibility.

FAK is required and sufficient for UPEC invasion. To further define the role of FAK in UTI, we overexpressed or silenced FAK in primary human urothelial cells and quantified bacterial attachment and invasion following UPEC challenge. FAK overexpression significantly increased UPEC invasion, while FAK silencing reduced invasion (**Figure 6A/B**). To test whether this effect is mediated by the downstream effector AKT, we overexpressed AKT and measured UPEC invasion**.** AKT overexpression had no impact on bacterial invasion, indicating that FAK promotes bacterial entry independent of AKT signaling **(Figure 6C).**

DISCUSSION:

Obesity is an established risk factor for infection, but the mechanisms underlying this increased susceptibility remain poorly defined (2-4, 27, 33). In this study, we demonstrate that diet-induced obesity increases UTI susceptibility and activates urothelial FAK signaling in both female and male mice. Using human urothelial cells, we show that FAK is both necessary and sufficient to drive UPEC invasion. These findings provide the first mechanistic link between obesity and UTI vulnerability, identifying FAK as a conserved and critical mediator of UPEC susceptibility in the obese bladder.

Our results build on clinical observations connecting obesity to increased UTI incidence and severity (4-11). While chronic inflammation and immune cell dysfunction have been proposed as contributing factors, direct mechanistic evidence is limited (2, 4, 34, 35). In our model, obesity did

not impact systemic inflammatory cytokines, impair phagocyte recruitment, or affect UPEC phagocytosis and killing, suggesting that enhanced susceptibility may be driven by other factors. Instead, we observed transcriptional remodeling in the urothelium, implicating uroepithelial vulnerability as a key contributor to UTI pathogenesis.

Obesity has been shown to disrupt epithelial integrity at mucosal surfaces, such as the lung, skin, reproductive tract, and gut (36, 37). In the bladder, we similarly identified sex-specific alterations in genes involved in barrier function and uroplakin plaque formation. In female mice, obesity suppressed several barrier-associated genes and uroplakin transcripts, while in male mice, many of these same genes were up-regulated. One possibility is that female urothelium is more transcriptionally sensitive to dietary fat exposure. Alternatively, male mice, which exhibit more pronounced metabolic dysfunction, may develop maladaptive remodeling programs in response to metabolic stress (2, 38). These findings point to metabolically driven deregulation of bladder urothelial structure and gene programs involved in epithelial maturation and barrier formation, albeit through sex-specific trajectories.

Hormonal signaling may be a key modulator of these effects. Insulin signaling, which is disrupted in obesity, is essential for maintaining epithelial integrity and immune responses (39-43). In prior work, we showed that insulin receptor deletion in the apical urothelium impairs barrier function and increases UTI severity – supporting a model in which metabolic cues influence epithelial remodeling (44). Sex hormones also influence the uroepithelium and UTI risk (45). Estrogen promotes urothelial differentiation and innate defense, while testosterone dampens immune responses during UTI (46-49). Consistent with these roles, female mice mount stronger IL-17-mediated responses and more effectively clear UPEC, whereas males are more prone to chronic infection (23, 30). These observations, together with our findings of sex-specific transcriptional responses with obesity, suggest that hormonal context shapes how the bladder urothelium responds to metabolic stress. Collectively, these data support a broader model in which metabolic

and hormonal signaling coordinate urothelial differentiation and host defense, and in which sex-based biological differences shape the bladder's response to both infection and obesity.

Consistent with this model of metabolic and hormonal regulation of bladder defense, our pathway analysis revealed shared up-regulation of focal adhesion, ECM-receptor interaction, and cytoskeletal signaling in both sexes. FAK, a central regulator of these pathways, was hyperactivated in urothelium of HFD-fed mice, facilitating UPEC invasion. Prior work using bladder cancer models has shown that UPEC exploits FAK signaling to trigger actin rearrangement and host cell entry, particularly through type 1 pili and the FimH adhesin, which engages with β1-integrins to activate FAK (50, 51). Our findings extend this mechanism to primary urothelial cells and provide the first direct evidence that FAK overexpression promotes UPEC infection. In contrast, inhibition of FAK, whether through genetic approaches or natural compounds, reduced UPEC internalization (50-54). Our *in vitro* results suggest that FAK is required, possibly through its downstream target MAPK, as overexpression of AKT alone could not drive bacterial invasion. These results position FAK as a key node integrating metabolic stress, epithelial remodeling, and microbial invasion.

An important and somewhat unexpected finding was the striking transcriptional divergence between male and female mice in response to obesity. Despite shared pathway enrichment, the differentially expressed genes were largely non-overlapping between male and female mice. This degree of divergence was surprising, as both sexes displayed increases in UTI susceptibility and FAK activation, suggesting a conserved phenotype despite distinct transcriptional programs. These differences likely reflect broader sex-based variation in metabolic and immune responses to obesity (27, 55-58). While the mechanistic links between obesity, immunity, and tissue-specific remodeling are still emerging, our findings suggest that obesity engages in sex-specific transcriptional pathways to drive a shared outcome of increased UPEC vulnerability. Moreover,

they highlight the importance of including both sexes in studies of UTI defense and support the development of sex-specific strategies for managing infection risk in the context of obesity.

This study has limitations. While the HFD model is well-suited for mechanistic investigation and mirrors key features of human obesity, it does not fully capture the complexity of human disease – including genetic, behavioral, and dietary variation (25, 26). Other obesogenic factors such as high sugar, salt, or saturated fat intake may exert distinct effects on immune and epithelial responses. Microbiota composition and environmental exposures could also influence host-pathogen interactions and UTI susceptibility (2, 59-61). Although we demonstrate a functional role for FAK *in vitro*, we have not yet tested whether pharmacologic inhibition of FAK *in vivo* can reduce bacterial burden or restore epithelial integrity in obesity. Finally, while we observed transcriptional changes in urothelial barrier genes, the precise relationship between FAK activation, urothelial differentiation, and epithelial remodeling remains to be defined. Future studies should investigate how metabolic and hormonal cues converge on FAK signaling to regulate bladder defense across diverse physiological and clinical contexts.

Despite these limitations, our study has strengths. We evaluated both male and female mice, revealing sex-specific transcriptional responses that are often overlooked in preclinical models of UTI and obesity (27). While few studies have examined immune function differences between males and females in the context of obesity, our findings highlight how obesity shapes urothelial and immune responses in a sex-dependent manner. By integrating *in vivo* UTI models, transcriptomics, and *in vitro* mechanistic assays, we provide a comprehensive view of how obesity disrupts bladder defense. This multifaceted approach provides a mechanistic framework linking metabolic stress to impaired bladder defense and supports the development for sex-specific therapeutic strategies to be implemented into clinical practice.

In conclusion, this study identifies focal adhesion signaling as a key pathway by which obesity increases UTI susceptibility. FAK integrates metabolic and mechanical cues to promote epithelial remodeling and UPEC invasion, making it a promising therapeutic target. Future work can explore whether modulating FAK activity can reduce infection burden in obesity. Understanding how metabolic and hormonal cues converge on epithelial signaling networks will be essential for developing precision strategies to protect at-risk patients.

MATERIALS AND METHODS:

Materials. Details of the reagents used can be found in **Supplemental Table 2**.

Mice. All mouse experiments were conducted in compliance with the rules and regulations of the Institutional Animal Care and Use Committee. Mice were housed under controlled temperature and humidity conditions, maintained on a 12-hour light-dark cycle, and were provided *ad libitum* access to rodent chow and water. Following weaning, mice were fed Teklad 6% fat standard chow (Inotiv, West Lafayette, IN, USA) until five to six weeks of age. Male and female C57BL/6 mice were then assigned to either a HFD consisting of 60% kilocalories from fat (Research Diets, Inc., New Brunswick, NJ, USA) or SC providing 10% kilocalories from fat (Research Diets). Mice were maintained on a HFD or SC for 4, 8, or 12 weeks.

Mouse Glucose Measurements and Cytokine Profiles. Blood glucose concentrations were obtained using AlphaTrak glucose monitoring system (Abbott Point of Care, Princeton, NJ, USA). Urinary glucose measurements were assessed by dipstick urinalysis (Chemstrip 2 GP, Roche, Basel, Switzerland). Glucose tolerance testing was performed following a six hour fast using established protocols (62). Blood glucose concentrations were measured using the AlphaTrak glucose monitoring system (Abbott Point of Care, Princeton, NJ, USA) at 15, 30, 60, and 90 minutes post injection of intraperitoneal D-glucose injection. The concentrations of 6 mouse

serum cytokines, including IFN-γ, IL-1β, IL-6, IL-10, IL-17A, and TNFα, were measured using a multiplex bead array platform (Bio-Plex, Bio-Rad, Hercules, CA).

Experimental UTI. Female mice were infected by transurethral catheterization with 10^7 colony-forming units (CFU) of UPEC (strain UTI89) following established protocols (43, 63). UTI89 is type 1-piliated UPEC strain isolated from a patient with cystitis.(64) Male mice were infected by direct bladder inoculation with 10^7 CFU of UTI89 (46). At the indicated time points, mice were anesthetized and sacrificed via cervical dislocation. Urine was collected, organs were aseptically harvested, and UPEC colonies were enumerated as previously described (43, 63).

Flow Cytometry. Bladders were harvested 24-hours after experimental UTI with GFP-expressing UTI89. Tissues were dissociated, single live cell suspensions were prepared, and stained for cell surface receptors with fluorescent monoclonal antibody combinations as previously published (**Supplemental Table 2**) (44, 65). UPEC+ cells were gated to enumerate phagocytosis by specific immune cell populations. Intracellular killing was evaluated by mean fluorescence intensity of intracellular GFP-UPEC. Stained cells were collected on a LSR II cytofluorometer (BD Biosciences, Franklin Lakes, NJ, USA) and data analyzed using the FlowJo software as previously published (Treestar, Ashland, TN, USA) (44).

PMN Isolation and *Ex vivo* UPEC Killing. Neutrophils were isolated from mouse femurs and tibias using the Mojosort Mouse Neutrophil Isolation Kit (BioLegend) following established protocols and were resuspended in RPMI medium with 10% fetal bovine serum (FBS, 2 x 10^5 cells/200μl) and placed in 96 well plates at 37°C (65, 66). PMNs were infected with UPEC at an MOI 100 or 1,000 at 37°C. After a 45 minute incubation, supernatants were collected after 45 minutes to assess the extracellular bacterial load. Samples were serially diluted and plated on LB Agar plates. UPEC CFUs were quantified the following day.

Urothelium Enrichment and RNA Sequencing. Bladders were aseptically harvested from mice maintained on either SC or HFD. Bladders were everted under a dissecting microscope using sterile forceps, then incubated at 37°C for 45 minutes in 2.5 mg/mL Dispase II (Thermo Fisher Scientific, Waltham, MA, USA) prepared in 50 mM HEPES/KOH pH 7.4 with 150 mM NaCl. The urothelium was then mechanically stripped from the detrusor muscle using sterile forceps (44). Isolated cells were washed with cold sterile phosphate buffered saline (PBS) and pelleted for RNA extraction. RNA was extracted using NucleoSpin RNA Plus XS Kit (Takara Bio, San Jose, CA, USA). RNA integrity was assessed using the Agilent Bioanalyzer 2100 (Agilent, Carlsbad, CA, USA). Samples with RNA integrity scores > 7 were submitted for sequencing.

For limiting-cell RNA-seq, RNA was pre-amplified using Clontech SMARTer v4 kit (Takara Bio) and cDNA libraries were generated using Nextera XT DNA Library Prep Kit (Illumina, San Diego, CA, USA). Samples were sequenced to 15 to 20 million paired-end (2 x 150 base pair) clusters on the Illumina HiSeq 4000 platform. Data processing and analysis were performed as previously described (67, 68). The reported sequences and metadata reported are deposited in the Gene Expression Omnibus (GEO) database (Accession No. GSE294660). Differentially expressed gene lists are provided as **Supplemental Dataset 1** (12 weeks on diet) and **Supplemental Dataset 2** (8 weeks on diet). RNA-seq analysis is outlined in the **Supplemental Methods**.

Cell Culture and Transfection. Primary human bladder urothelial cells (HBLAK), obtained from an 80-year old male, were purchased from CELLnTEC Advanced Cell Systems and grown in CELLnTEC CnT-Prime Epithelial Proliferation Medium (CELLnTEC, Bern, Switzerland) (69, 70). Cells were cultured at 37°C and 5% CO_2. Transfection experiments were initiated when cells approached 95% confluency. **siRNA Transfection**: Pooled siRNA libraries targeting human *PTK2* and a non-targeting pool (negative control) were purchased (**Supplemental Table 2**). Cells were transfected with a mixture of siRNA, DharmaFECT transfection reagent (Horizon Discovery,

Waterbeach, UK), and culture media per the manufacturer's recommendations. Seventy-two hours after transfection, cells lysates were collected for Western blot or UPEC attachment and invasion assays were performed. **Retrovirus Transduction**: FAK was overexpressed by retroviral transduction of cells with pWZL-Neo-Myr_Flag-DEST (empty control) or pWZL-Neo-Myr-Flag-PTK2 (Addgene, Watertown, MA, USA) (71). Retrovirus was produced using Phoenix-AMPHO cells (ATCC, Manassas, VA, USA). **Plasmid Transfection**: AKT was overexpressed by transfecting cells with 500 ng pCMV5-hemagglutinin (HA)-PKBα (WT) or pCMV5-HA-membrane targeted-PKBα (M/P) (purchased from D. Alessi, University of Dundee, Dundee, United Kingdom) using Lipofectamine 2000 according to the manufacturer's instructions (Thermo Fisher Scientific, Waltham, MA, USA) (72). For all experiments, culture media was changed 16 hours after transfection or transduction. Experiments were performed 72 hours post transfection or transduction.

***In vitro* UPEC Infection Assays.** UPEC attachment and invasion assays were performed as previously described using HBLAK cells (44, 73). Seventy-two hours following transfection or transduction, cells were infected with 10 multiplicity of infection (MOI) UTI89. After 2 hours, one set of wells was lysed in 0.1% Triton X-100 to enumerate total UPEC per well (extracellular and intracellular). To define UPEC invasion, a second set of wells were incubated in culture medium supplemented with gentamicin to kill extracellular bacteria. After 3 hours, cells were washed and lysed to evaluate bacterial invasion. Lysates were plated and bacterial CFUs were enumerated after overnight growth on LB agar. The percentage of intracellular bacteria was calculated as the number of UPEC recovered divided by the total number of UPEC (44, 73).

Western Blotting and Quantification. Mouse urothelium, total bladder, and HBLAK tissue culture lysates were prepared by homogenizing tissue or cells in RIPA buffer (25 mM Tris-HCl, pH 7.6; 150 mM NaCl, 1% NP-40, 1% sodium deoxycholate, 1% sodium dodecyl sulfate)

supplemented with protease and phosphatase inhibitor (Thermo Fisher Scientific, Waltham, MA, USA). Western blot was performed as previously described (73). Antibodies directed against the following targets were used P-FAK (Y397), P-AKT (S473), GAPDH (Cell Signaling, Danvers, MA, USA); M2-FLAG tag, HA tag (Sigma Aldrich, Burlingame, MA, USA). Quantitation of Western blot intensity was performed using ImageLab software (Bio-Rad, Hercules, CA, USA). Relative expression was determined by dividing the background-corrected intensity of P-FAK or P-AKT band by the background-corrected intensity of corresponding GAPDH band.

Immunostaining and Microscopy. Immunofluorescent staining was performed using published methods (44, 73). Bladders were labeled with a rabbit anti-FAK antibody (Abcam, Waltham, MA, USA), polyclonal goat anti-Uroplakin 3 (Upk3) antibody (Santa Cruz Biotechnology, Dallas, TX, USA). Alexa Fluor® 488 AffiniPure donkey anti-goat IgG and Cy™3 AffiniPure $F(ab')_2$ fragment donkey anti-rabbit IgG served as secondary antibodies (Jackson ImmunoResearch Laboratories, West Grove, PA, USA). Nuclei were labeled using Hoechst (Thermo Fisher Scientific, Waltham, MA, USA). Microscopy images were captured using a Nikon Ti2-E microscope and DS-RI2 camera (Nikon Instruments Inc., Melville, NY, USA).

STATISTICAL ANALYSIS: Continuous differences between groups were evaluated for a normal distribution with the D'Agostino-Pearson Omnibus or Shapiro-Wilk normality test, with normality defined as a *P*-value > 0.05. Comparisons on normally distributed data were performed using a Student's *t*-test or ANOVA; otherwise, the nonparametric Mann-Whitney *U* or Kruskal-Wallis tests were used. Data from *in vitro* experiments were normally distributed and are presented as means +/- SEM. Differences between groups with a *P*-value < 0.05 were considered statistically significant.

Acknowledgments: We thank Birong (Rollin) Li in the Kidney and Urinary Tract Center at the Abigail Wexner Research Institute at Nationwide Children's Hospital for assistance with the

mouse infections. This work is supported by the National Institutes of Health (NIDDK) R01 DK114035 and R01 DK128088 (J.D.S.) and K01 DK128379 (J.R-R.). Limiting-cell RNA-seq was performed at The Ohio State University Comprehensive Cancer Center's Genomics Shared Resource which is supported by a Comprehensive Cancer Support Grant P30CA016058.

REFERENCES:

1. C. L. Ogden, M. D. Carroll, B. K. Kit, K. M. Flegal, Prevalence of childhood and adult obesity in the United States, 2011-2012. *JAMA* **311**, 806-814 (2014).
2. S. R. Shaikh, M. A. Beck, Y. Alwarawrah, N. J. MacIver, Emerging mechanisms of obesity-associated immune dysfunction. *Nat Rev Endocrinol* **20**, 136-148 (2024).
3. I. Lingvay, R. V. Cohen, C. W. L. Roux, P. Sumithran, Obesity in adults. *Lancet* **404**, 972-987 (2024).
4. G. Pugliese *et al.*, Obesity and infectious diseases: pathophysiology and epidemiology of a double pandemic condition. *Int J Obes (Lond)* **46**, 449-465 (2022).
5. M. E. Falagas, M. Kompoti, Obesity and infection. *Lancet Infect Dis* **6**, 438-446 (2006).
6. M. J. Semins, A. D. Shore, M. A. Makary, J. Weiner, B. R. Matlaga, The impact of obesity on urinary tract infection risk. *Urology* **79**, 266-269 (2012).
7. W. Nseir *et al.*, Obesity and recurrent urinary tract infections in premenopausal women: a retrospective study. *Int J Infect Dis* **41**, 32-35 (2015).
8. W. R. Grier, P. Kratimenos, S. Singh, J. P. Guaghan, I. Koutroulis, Obesity as a Risk Factor for Urinary Tract Infection in Children. *Clin Pediatr (Phila)* **55**, 952-956 (2016).
9. P. C. Hsu, S. J. Chen, Obesity and risk of urinary tract infection in young children presenting with fever. *Medicine (Baltimore)* **97**, e13006 (2018).
10. M. C. Harpsoe *et al.*, Body Mass Index and Risk of Infections Among Women in the Danish National Birth Cohort. *Am J Epidemiol* **183**, 1008-1017 (2016).
11. A. Mahyar *et al.*, The role of overweight and obesity in urinary tract infection in children. *Infez Med* **24**, 38-42 (2016).
12. W. Saliba, O. Barnett-Griness, G. Rennert, The association between obesity and urinary tract infection. *Eur J Intern Med* **24**, 127-131 (2013).
13. F. Ghilotti, R. Bellocco, W. Ye, H. O. Adami, Y. Trolle Lagerros, Obesity and risk of infections: results from men and women in the Swedish National March Cohort. *Int J Epidemiol* **48**, 1783-1794 (2019).
14. B. Wurzinger *et al.*, The association between body-mass index and patient outcome in septic shock: a retrospective cohort study. *Wien Klin Wochenschr* **122**, 31-36 (2010).
15. G. V. Bochicchio *et al.*, Impact of obesity in the critically ill trauma patient: a prospective study. *J Am Coll Surg* **203**, 533-538 (2006).
16. Y. Okubo, A. Handa, The impact of obesity on pediatric inpatients with urinary tract infections in the United States. *J Pediatr Urol* **13**, 455 e451-455 e455 (2017).
17. T. H. Yang, H. E. Yim, K. H. Yoo, Obesity and a febrile urinary tract infection: dual burden for young children? *Urology* **84**, 445-449 (2014).
18. T. S. Antonelli *et al.*, Body fat predicts urinary tract infection in kidney transplant recipients: a prospective cohort study. *J Nephrol* **37**, 1551-1562 (2024).
19. J. B. Kaper, J. P. Nataro, H. L. Mobley, Pathogenic Escherichia coli. *Nat Rev Microbiol* **2**, 123-140 (2004).
20. M. G. Dalghi, N. Montalbetti, M. D. Carattino, G. Apodaca, The Urothelium: Life in a Liquid Environment. *Physiol Rev* **100**, 1621-1705 (2020).
21. B. Becknell, A. Schwaderer, D. S. Hains, J. D. Spencer, Amplifying renal immunity: the role of antimicrobial peptides in pyelonephritis. *Nat Rev Nephrol* **11**, 642-655 (2015).
22. L. Schwartz, J. de Dios Ruiz-Rosado, E. Stonebrook, B. Becknell, J. D. Spencer, Uropathogen and host responses in pyelonephritis. *Nat Rev Nephrol* 10.1038/s41581-023-00737-6 (2023).
23. L. Lacerda Mariano, M. A. Ingersoll, The immune response to infection in the bladder. *Nat Rev Urol* **17**, 439-458 (2020).
24. A. J. Lewis, A. C. Richards, M. A. Mulvey, Invasion of Host Cells and Tissues by Uropathogenic Bacteria. *Microbiol Spectr* **4** (2016).

25. E. D. M. de Moura *et al.*, Diet-induced obesity in animal models: points to consider and influence on metabolic markers. *Diabetol Metab Syndr* **13**, 32 (2021).
26. A. M. Svensson, C. Hellerstrom, L. Jansson, Diet-induced obesity and pancreatic islet blood flow in the rat: a preferential increase in islet blood perfusion persists after withdrawal of the diet and normalization of body weight. *J Endocrinol* **151**, 507-511 (1996).
27. J. R. Braga Tibaes *et al.*, Sex differences in systemic inflammation and immune function in diet-induced obesity rodent models: A systematic review. *Obes Rev* **25**, e13665 (2024).
28. Y. Yang, D. L. Smith, Jr., K. D. Keating, D. B. Allison, T. R. Nagy, Variations in body weight, food intake and body composition after long-term high-fat diet feeding in C57BL/6J mice. *Obesity (Silver Spring)* **22**, 2147-2155 (2014).
29. M. S. Islam, V. Venkatesan, Experimentally-Induced Animal Models of Prediabetes and Insulin Resistance: A Review. *Acta Pol Pharm* **73**, 827-834 (2016).
30. A. Zychlinsky Scharff *et al.*, Sex differences in IL-17 contribute to chronicity in male versus female urinary tract infection. *JCI Insight* **5** (2019).
31. X. Tan *et al.*, Focal adhesion kinase: from biological functions to therapeutic strategies. *Exp Hematol Oncol* **12**, 83 (2023).
32. D. D. Schlaepfer, C. R. Hauck, D. J. Sieg, Signaling through focal adhesion kinase. *Prog Biophys Mol Biol* **71**, 435-478 (1999).
33. A. Ray, M. J. L. Bonorden, R. Pandit, K. J. Nkhata, A. Bishayee, Infections and immunity: associations with obesity and related metabolic disorders. *J Pathol Transl Med* **57**, 28-42 (2023).
34. C. J. Andersen, K. E. Murphy, M. L. Fernandez, Impact of Obesity and Metabolic Syndrome on Immunity. *Adv Nutr* **7**, 66-75 (2016).
35. C. T. de Andrade, G. Z. Rocha, M. Zamuner, R. B. Dos Reis, L. O. Reis, Obesity influence on bladder inflammation and cancer: a cystitis model. *Int J Clin Exp Pathol* **15**, 373-379 (2022).
36. Y. Pat *et al.*, Recent advances in the epithelial barrier theory. *Int Immunol* **36**, 211-222 (2024).
37. D. Statovci, M. Aguilera, J. MacSharry, S. Melgar, The Impact of Western Diet and Nutrients on the Microbiota and Immune Response at Mucosal Interfaces. *Front Immunol* **8**, 838 (2017).
38. A. R. Saltiel, J. M. Olefsky, Inflammatory mechanisms linking obesity and metabolic disease. *J Clin Invest* **127**, 1-4 (2017).
39. S. F. Andres *et al.*, Deletion of intestinal epithelial insulin receptor attenuates high-fat diet-induced elevations in cholesterol and stem, enteroendocrine, and Paneth cell mRNAs. *Am J Physiol Gastrointest Liver Physiol* **308**, G100-111 (2015).
40. S. Tsai *et al.*, Insulin Receptor-Mediated Stimulation Boosts T Cell Immunity during Inflammation and Infection. *Cell Metab* **28**, 922-934 e924 (2018).
41. T. Senokuchi *et al.*, Forkhead transcription factors (FoxOs) promote apoptosis of insulin-resistant macrophages during cholesterol-induced endoplasmic reticulum stress. *Diabetes* **57**, 2967-2976 (2008).
42. E. Ieronymaki *et al.*, Insulin Resistance in Macrophages Alters Their Metabolism and Promotes an M2-Like Phenotype. *J Immunol* **202**, 1786-1797 (2019).
43. M. J. Murtha *et al.*, Insulin receptor signaling regulates renal collecting duct and intercalated cell antibacterial defenses. *J Clin Invest* **128**, 5634-5646 (2018).
44. L. Schwartz *et al.*, Insulin receptor signaling engages bladder urothelial defenses that limit urinary tract infection. *Cell Rep* **43**, 114007 (2024).
45. L. Deltourbe, L. Lacerda Mariano, T. N. Hreha, D. A. Hunstad, M. A. Ingersoll, The impact of biological sex on diseases of the urinary tract. *Mucosal Immunol* **15**, 857-866 (2022).
46. P. D. Olson *et al.*, Androgen exposure potentiates formation of intratubular communities and renal abscesses by Escherichia coli. *Kidney Int* **94**, 502-513 (2018).

47. C. D. Albracht, T. N. Hreha, D. A. Hunstad, Sex effects in pyelonephritis. *Pediatr Nephrol* **36**, 507-515 (2021).
48. P. Luthje *et al.*, Estrogen supports urothelial defense mechanisms. *Sci Transl Med* **5**, 190ra180 (2013).
49. P. D. Olson, K. A. Hruska, D. A. Hunstad, Androgens Enhance Male Urinary Tract Infection Severity in a New Model. *J Am Soc Nephrol* **27**, 1625-1634 (2016).
50. J. J. Martinez, M. A. Mulvey, J. D. Schilling, J. S. Pinkner, S. J. Hultgren, Type 1 pilus-mediated bacterial invasion of bladder epithelial cells. *EMBO J* **19**, 2803-2812 (2000).
51. D. S. Eto, T. A. Jones, J. L. Sundsbak, M. A. Mulvey, Integrin-mediated host cell invasion by type 1-piliated uropathogenic Escherichia coli. *PLoS Pathog* **3**, e100 (2007).
52. W. J. Kim, A. E. Shea, J. H. Kim, Y. Daaka, Uropathogenic Escherichia coli invades bladder epithelial cells by activating kinase networks in host cells. *J Biol Chem* **293**, 16518-16527 (2018).
53. A. J. Lewis *et al.*, Plant phenolics inhibit focal adhesion kinase and suppress host cell invasion by uropathogenic Escherichia coli. *Infect Immun* **92**, e0008024 (2024).
54. P. Luthje, D. N. Dzung, A. Brauner, Lactuca indica extract interferes with uroepithelial infection by Escherichia coli. *J Ethnopharmacol* **135**, 672-677 (2011).
55. L. T. Schuetz *et al.*, Sex differentially affects pro-inflammatory cell subsets in adipose tissue depots in a diet induced obesity model. *Biol Sex Differ* **15**, 105 (2024).
56. R. Ter Horst *et al.*, Sex-Specific Regulation of Inflammation and Metabolic Syndrome in Obesity. *Arterioscler Thromb Vasc Biol* **40**, 1787-1800 (2020).
57. J. M. Poret, D. A. Gaudet, H. D. Braymer, S. D. Primeaux, Sex differences in markers of metabolic syndrome and adipose tissue inflammation in obesity-prone, Osborne-Mendel and obesity-resistant, S5B/Pl rats. *Life Sci* **273**, 119290 (2021).
58. K. Karastergiou, S. R. Smith, A. S. Greenberg, S. K. Fried, Sex differences in human adipose tissues - the biology of pear shape. *Biol Sex Differ* **3**, 13 (2012).
59. C. D. Davis, The Gut Microbiome and Its Role in Obesity. *Nutr Today* **51**, 167-174 (2016).
60. T. E. Adolph, H. Tilg, Western diets and chronic diseases. *Nat Med* **30**, 2133-2147 (2024).
61. B. N. Liu, X. T. Liu, Z. H. Liang, J. H. Wang, Gut microbiota in obesity. *World J Gastroenterol* **27**, 3837-3850 (2021).
62. Anonymous (https://www.diacomp.org/shared/document.aspx?id=11&docType=Protocol.
63. C. S. Hung, K. W. Dodson, S. J. Hultgren, A murine model of urinary tract infection. *Nat Protoc* **4**, 1230-1243 (2009).
64. M. A. Mulvey, J. D. Schilling, S. J. Hultgren, Establishment of a persistent Escherichia coli reservoir during the acute phase of a bladder infection. *Infect Immun* **69**, 4572-4579 (2001).
65. J. D. Ruiz-Rosado *et al.*, Neutrophil-Macrophage Imbalance Drives the Development of Renal Scarring during Experimental Pyelonephritis. *J Am Soc Nephrol* **32**, 69-85 (2021).
66. I. Cotzomi-Ortega *et al.*, Neutrophil NADPH oxidase promotes bacterial eradication and regulates NF-kappaB-Mediated inflammation via NRF2 signaling during urinary tract infections. *Mucosal Immunol* 10.1016/j.mucimm.2024.12.010 (2024).
67. L. A. Walker *et al.*, CLEAR: coverage-based limiting-cell experiment analysis for RNA-seq. *J Transl Med* **18**, 63 (2020).
68. L. Schwartz *et al.*, Insulin receptor orchestrates kidney antibacterial defenses. *Proc Natl Acad Sci U S A* **121**, e2400666121 (2024).
69. H. Horsley, D. Dharmasena, J. Malone-Lee, J. L. Rohn, A urine-dependent human urothelial organoid offers a potential alternative to rodent models of infection. *Sci Rep* **8**, 1238 (2018).
70. M. J. Hoffmann *et al.*, The New Immortalized Uroepithelial Cell Line HBLAK Contains Defined Genetic Aberrations Typical of Early Stage Urothelial Tumors. *Bladder Cancer* **2**, 449-463 (2016).

71. J. S. Boehm *et al.*, Integrative genomic approaches identify IKBKE as a breast cancer oncogene. *Cell* **129**, 1065-1079 (2007).
72. M. Andjelkovic *et al.*, Role of translocation in the activation and function of protein kinase B. *J Biol Chem* **272**, 31515-31524 (1997).
73. K. Bender *et al.*, Expression and function of human ribonuclease 4 in the kidney and urinary tract. *Am J Physiol Renal Physiol* **320**, F972-F983 (2021).

Figures and Figure Legends

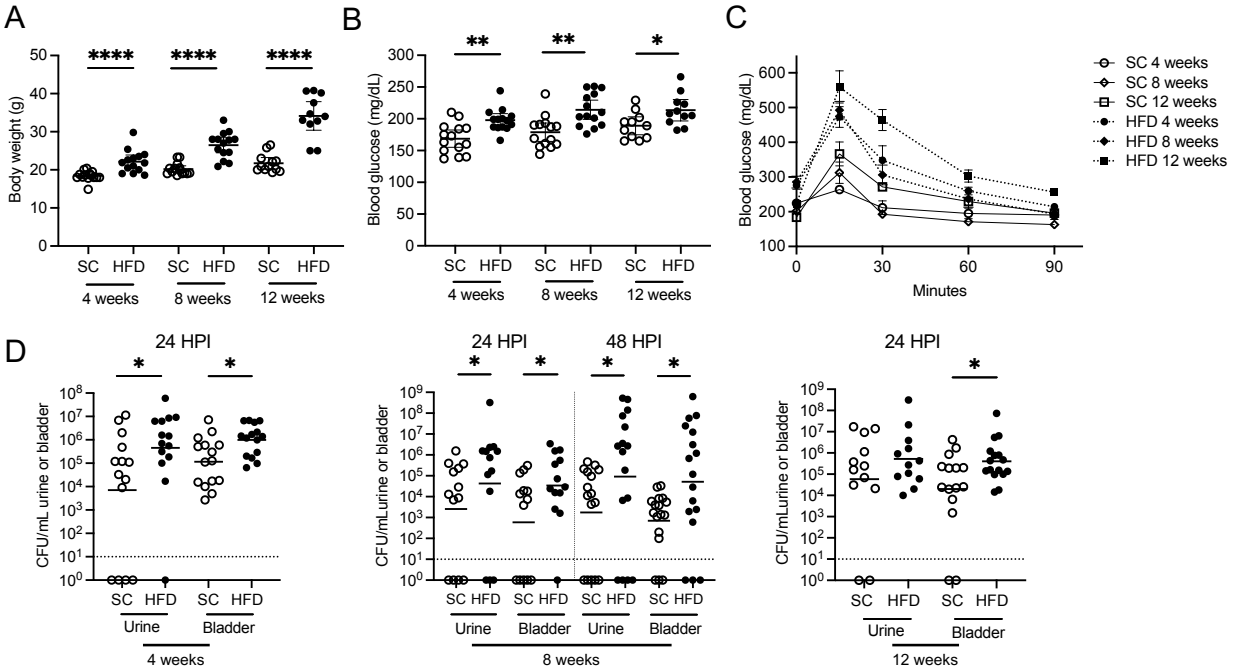

Figure 1: Obesity increases susceptibility to uropathogenic *E. coli* in female mice.
(**A-C**) Body weight (A), non-fasting blood glucose (B), and blood glucose concentrations following intraperitoneal glucose tolerance testing (C) measured in female C57/BL6 mice maintained on standard chow (SC) or a high-fat diet (HFD) for 4, 8, or 12 weeks. Graphs show the mean values and SEM. (**D**) Urine and bladder UPEC (UTI89) burden enumerated after transurethral UTI at the indicated time points. HPI notes hours post infection. The horizontal line indicates the geometric mean of each group. The dotted line indicates the limits of detection. (A-D) Each data point represents a measurement from an individual animal. Asterisks indicate significant *P*-values for the indicated pairwise comparison (Mann-Whitney *U* test). **P* <0.05, ***P* <0.01, and *****P* <0.0001.

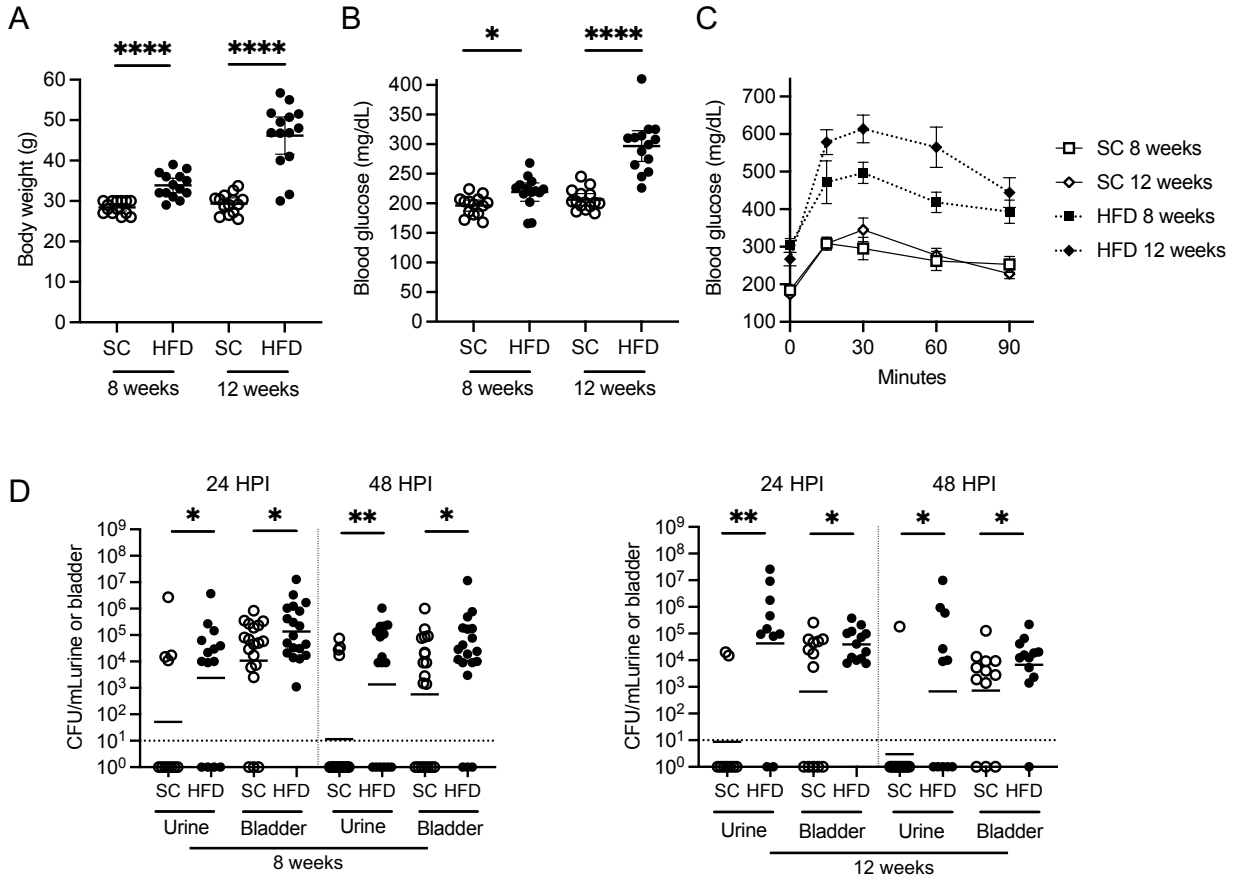

Figure 2: Obesity increases susceptibility to uropathogenic *E. coli* in male mice.
(**A-C**) Body weight (A), non-fasting blood glucose (B), and blood glucose concentrations following intraperitoneal glucose tolerance testing (C) measured in male C57/BL6 mice maintained on standard chow (SC) or a high-fat diet (HFD) for 8 or 12 weeks. Graphs show the mean values and SEM. (**D**) Urine and bladder UPEC (UTI89) burden enumerated after direct bladder inoculation at the indicated time points. HPI notes hours post infection. The horizontal line indicates the geometric mean of each group. The dotted line indicates the limits of detection. (A-D) Each data point represents a measurement from an individual animal. Asterisks indicate significant *P*-values for the indicated pairwise comparison (Mann-Whitney *U* test). **P* <0.05, ***P* <0.01, and *****P* <0.0001.

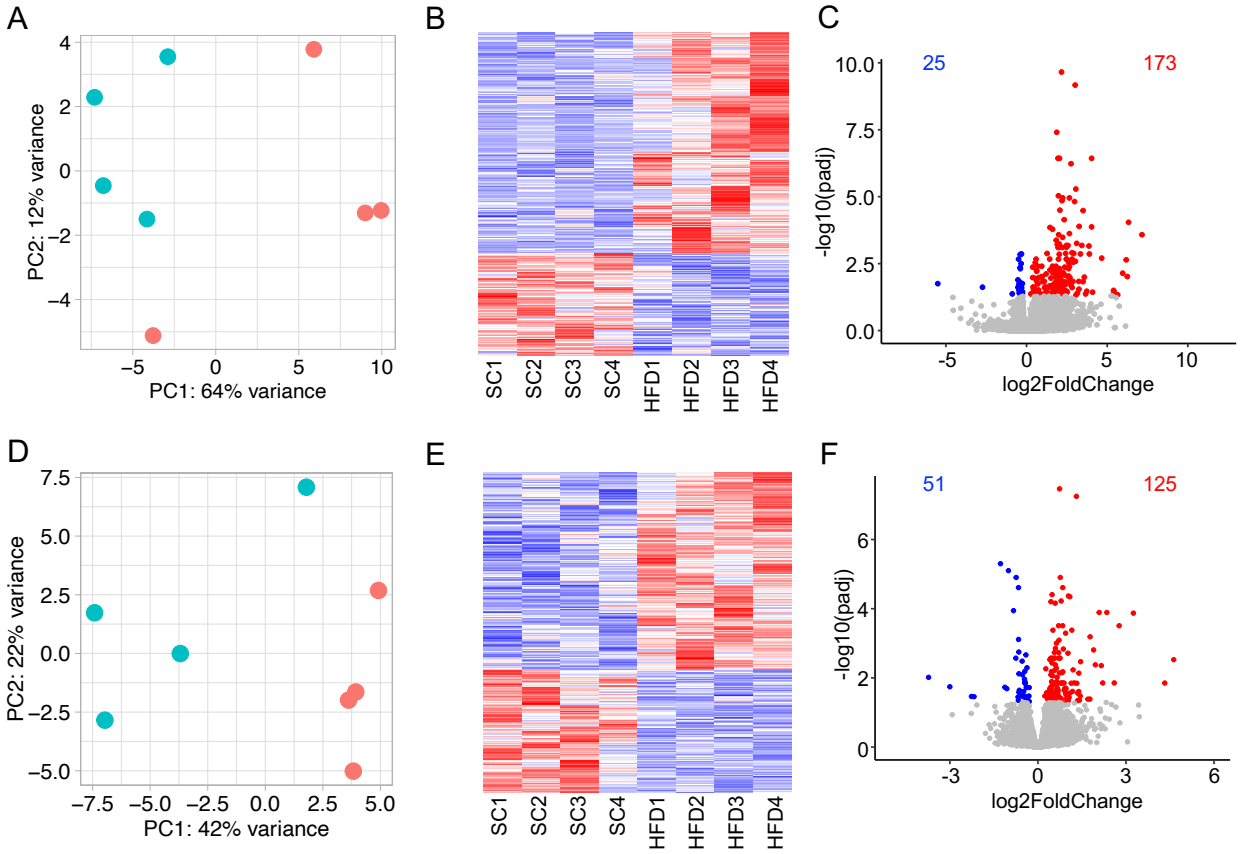

Figure 3: Obesity alters gene expression in the female and male urothelium. (**A/D**) Principal component analysis (PCA) plots from RNA-seq data of female (A) and male (D) urothelium after 12 weeks on standard chow (SC) or high-fat diet (HFD). Each symbol represents a urothelial sample from an individual mouse fed SC (green) or HFD (red). (**B**/**E**) Heatmaps showing differential gene expression between HFD and SC fed female (B) and male (E) urothelium, with each column representing an individual mouse. (**C**/**F**) Volcano plots illustrating differentially expressed genes expression between HFD and SC fed female (C) and male (F) urothelium. Red marks up-regulated genes with log2 fold change > 0 and adjusted *P*-value < 0.05. Blue marks down-regulated genes with log2 fold change < 0 and adjusted *P*-value < 0.05. Adjusted *P*-values were calculated using the Benjamini-Hochberg procedure.

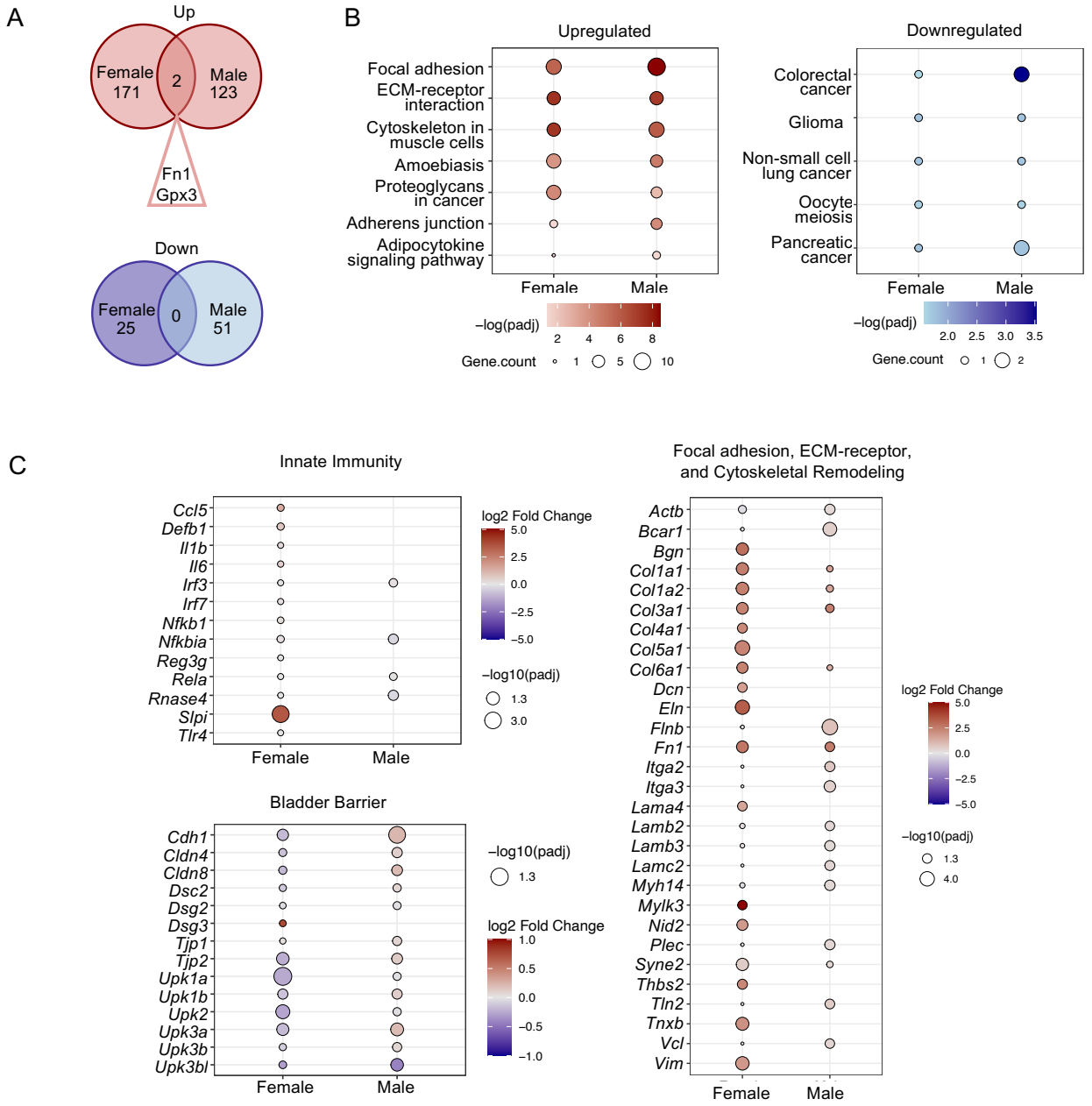

Figure 4: Obesity increases cell-ECM signaling in the urothelium. (**A**) Venn diagrams show minimal overlap between significantly up-regulated (top) and down-regulated (bottom) genes in female and male urothelium after 12 weeks on standard chow (SC) or high-fat diet (HFD). (**B**) KEGG pathway enrichment derived from up-regulated (left) and down-regulated (right) genes in HFD-fed female and male mice. Bubble size reflects the number of enriched genes per pathway and color indicates significance. (**C**) Expression of curated gene sets related to innate immunity, bladder barrier integrity, and focal adhesion/ECM/cytoskeletal remodeling. Bubble color represents log2 fold change (HFD vs. SC) and size indicates significance. (B-C) Significance was assessed via hypergeometric testing on active subnetworks identified from the protein-protein interaction network using PathfindR, with *P*-values adjusted using the Benjamini-Hochberg method.

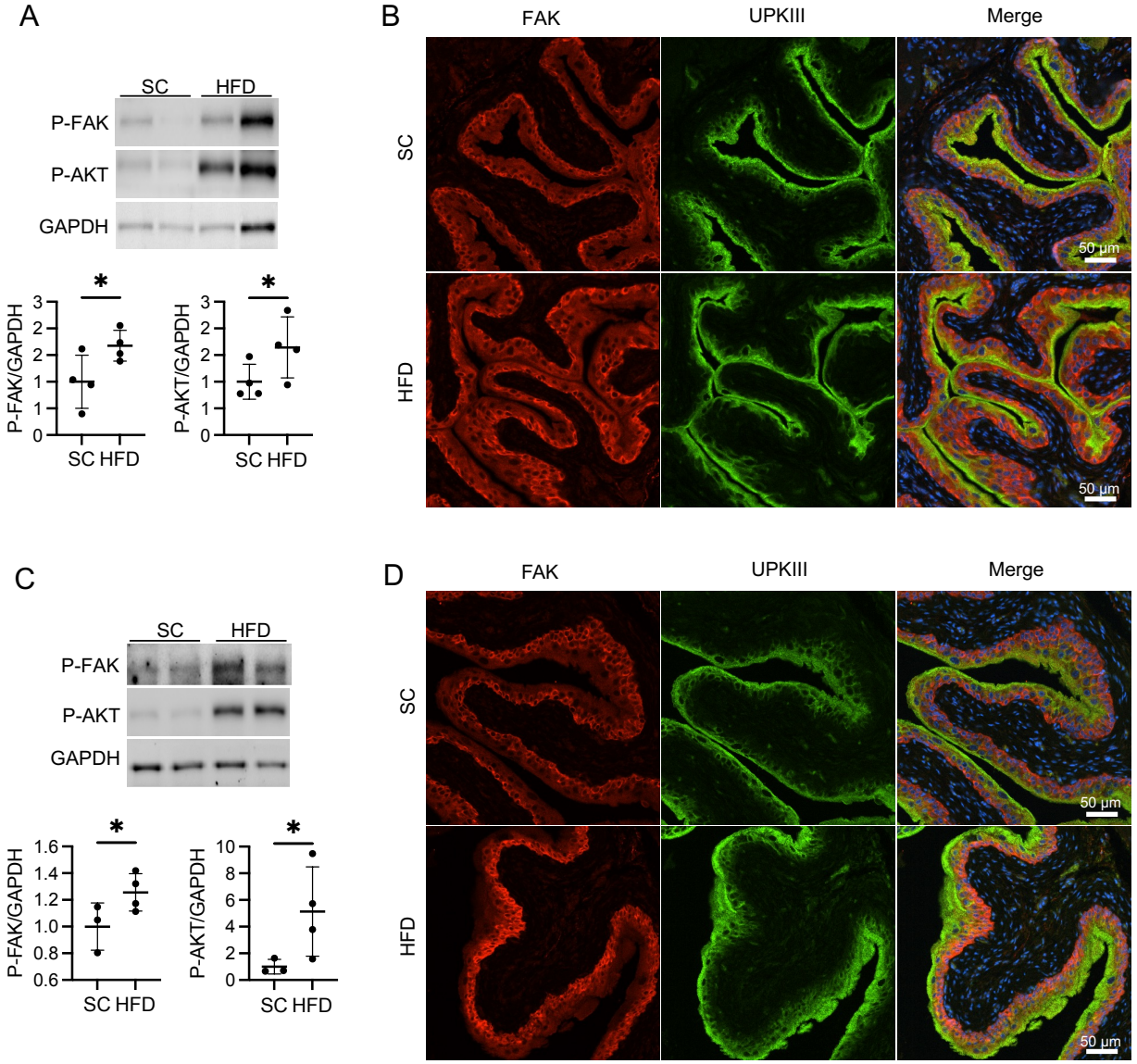

Figure 5: High-fat diet increases focal adhesion kinase activation in the bladder urothelium. (**A**/**C**) Representative Western blots from (A) female and (C) male urothelium after 8 weeks on standard chow (SC) or high-fat diet (HFD) probed for P-FAK (Y397), P-AKT (S473), and GAPDH. Bottom: Densitometry show relative abundance of P-FAK (Y397) and P-AKT (S473), normalized to GAPDH. Each point represents an individual mouse (*n*=4/cohort). Graphs show the mean and standard deviation. Statistical significance was assessed using the Mann-Whitney *U* test. **P* <0.05. (**B**/**D**) Representative immunofluorescent bladder images from non-infected (B) female and (D) male mice labeled with antibodies to total FAK (red), uroplakin III (green) and nuclei (blue, Hoechst). Magnification = 20X. Staining was completed on 4 bladders per cohort.

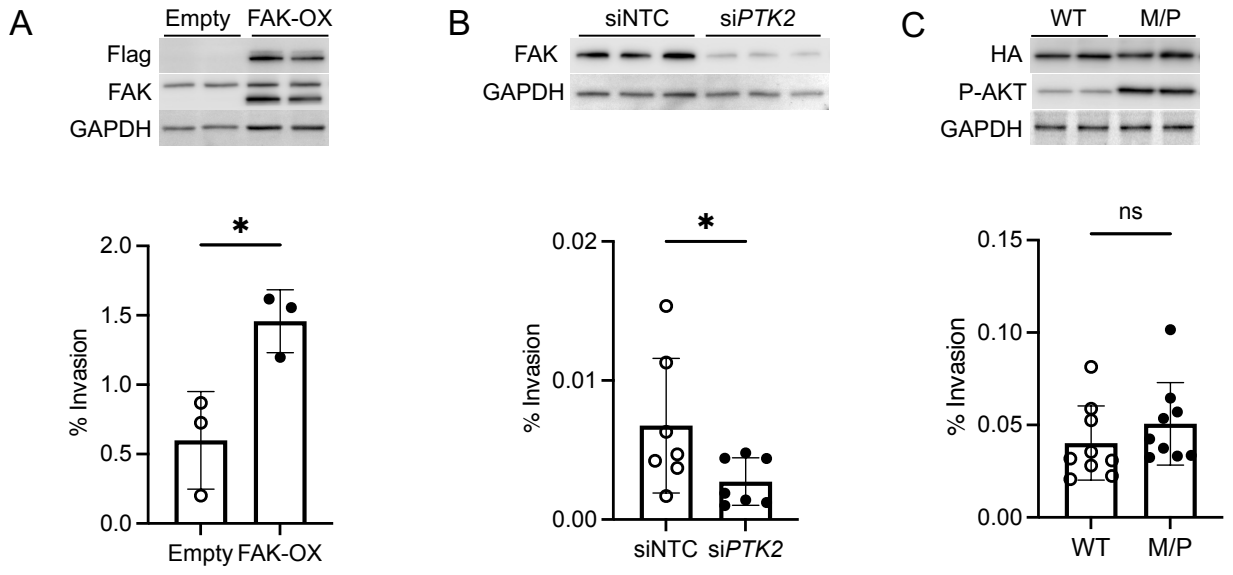

Figure 6: FAK is both required and sufficient for UPEC invasion of human urothelial cells. (**A**) Human bladder urothelial cells were transfected with empty vector (Empty) or Flag-tagged FAK (FAK-OX). Top: Representative Western blot confirmed increased Flag tag expression FAK expression in FAK-OX cells. Bottom: Transfected cells were challenged with UPEC. Shown are the percentage of bacteria invading the cells. (**B**) Human urothelial cells were transfected with non-targeting siRNA control (siNTC) or PTK2-targeting siRNA (siPTK2), which encodes FAK. Top: Representative Western blot confirmed FAK knockdown. Bottom: Transfected cells were challenged with UPEC and the percentage of invading UPEC are shown. (**C**) Human urothelial cells were transfected with HA-tagged wild-type AKT (WT) or membrane-targeted AKT (M/P). Top: Representative Western blot confirmed HA tag expression and increased P-AKT expression. Bottom: Transfected cells were challenged with UPEC and shown and the percentage of invading UPEC are shown. (A-C) Graphs show the mean and SEM. Results are from 3-9 independent experiments performed in triplicate (n=3-9). Asterisks indicate significant P-values (Student's t-test). *P <0.05.

Supplemental Methods

Mouse Limiting Cell RNA-seq Analysis

RNA-seq data preprocessing, alignment, and quantification: Individual FASTQ files were trimmed for adapter sequences and filtered for a minimum Phred quality score of Q20 using Adapter Removal v2.2.0 – indicating that the base call accuracy is 99% or greater (1). Preliminary alignment was performed using HISAT2 to a composite reference of ribosomal RNA, mitochondrial DNA, and PhiX bacteriophage sequences obtained from National Center for Biotechnology Information Reference Sequence Database (RefSeq) (2). Reads aligning to these references were excluded in subsequent analyses. Primary alignment was performed against the mouse genome reference GRCm38p4 using HISAT2 alignment program. Gene expression values for genes described by the GENCODE Gene Transfer Format release M14 were quantified using the featureCounts tool of the Subread package in unstranded mode (3-6).

Sequencing and alignment quality control: Quality control was performed using a modification of the QuaCRS custom workflow (7). In brief, aligned read quality was verified using RNA-SeQC and RSeQC (8, 9). The exonic rate (the percentage of reads aligning to exons), intronic rate (the percentage of reads aligning to introns), and duplication rate (the percentage of reads that were identified as PCR duplicates) were evaluated.

Coverage profiling: Coverage depths across the aligned reference were calculated with a per-base resolution using the 'genomecov' utility of Bedtools in BedGraph format (10). These files were used as input into CLEAR: a gene-by-gene analysis workflow to identify genes in ultra-low input RNA-seq data for downstream analyses. Determination of analysis-ready CLEAR transcripts was performed as previously described (11).

RNA-Seq data analysis: Principal component analysis (PCA) visualized differences between samples. All PCA plots were generated from counts tables that were size-normalized and r-log

transformed after CLEAR selection using methods included with DESeq2. Comparisons were processed using plotPCA and visualized using ggplot (12-14). Differentially expressed genes were called using DESeq2 from CLEAR counts tables generated with featureCounts as described above (12). In all figures, a false discovery rate *q*-value of < 0.05 was used as the inclusion criterion for differentially expressed genes (DEGs). DEGs were visualized by volcano plot generated using ggplot.

Venn diagram analysis: Overlapping upregulated or downregulated DEGs from female and male mice were determined using Biovenn (15). Venn diagrams were made in Microsoft PowerPoint.

KEGG pathway analysis: PathfindR was used to identify KEGG pathways enriched from DEGs with adjusted *P*-value < 0.05.(16) Upregulated genes (log2FoldChange > 0) and downregulated (log2FoldChange < 0) DEGs were used as input, separately. Pathway enrichment was reported as a bubble plot made using ggplot; size of bubbles represented the number of DEGs in each term and color represented *P*-value of enrichment. Differential expression of individual genes within KEGG terms were visualized by bubble plot generated using ggplot.

Supplemental References

1. M. Schubert, S. Lindgreen, L. Orlando, AdapterRemoval v2: rapid adapter trimming, identification, and read merging. *BMC Res Notes* **9**, 88 (2016).
2. N. A. O'Leary *et al.*, Reference sequence (RefSeq) database at NCBI: current status, taxonomic expansion, and functional annotation. *Nucleic Acids Res* **44**, D733-745 (2016).
3. J. Harrow *et al.*, GENCODE: producing a reference annotation for ENCODE. *Genome Biol* **7 Suppl 1**, S4 1-9 (2006).
4. J. Harrow *et al.*, GENCODE: the reference human genome annotation for The ENCODE Project. *Genome Res* **22**, 1760-1774 (2012).
5. Y. Liao, G. K. Smyth, W. Shi, The Subread aligner: fast, accurate and scalable read mapping by seed-and-vote. *Nucleic Acids Res* **41**, e108 (2013).
6. Y. Liao, G. K. Smyth, W. Shi, featureCounts: an efficient general purpose program for assigning sequence reads to genomic features. *Bioinformatics* **30**, 923-930 (2014).
7. K. W. Kroll *et al.*, Quality Control for RNA-Seq (QuaCRS): An Integrated Quality Control Pipeline. *Cancer Inform* **13**, 7-14 (2014).
8. D. S. DeLuca *et al.*, RNA-SeQC: RNA-seq metrics for quality control and process optimization. *Bioinformatics* **28**, 1530-1532 (2012).
9. L. Wang, S. Wang, W. Li, RSeQC: quality control of RNA-seq experiments. *Bioinformatics* **28**, 2184-2185 (2012).
10. A. R. Quinlan, I. M. Hall, BEDTools: a flexible suite of utilities for comparing genomic features. *Bioinformatics* **26**, 841-842 (2010).
11. L. A. Walker *et al.*, CLEAR: coverage-based limiting-cell experiment analysis for RNA-seq. *J Transl Med* **18**, 63 (2020).
12. M. I. Love, W. Huber, S. Anders, Moderated estimation of fold change and dispersion for RNA-seq data with DESeq2. *Genome Biol* **15**, 550 (2014).
13. H. Wickham, *ggplot2: Elegant Graphics for Data Analysis* (Springer-Verlag New York, 2016).
14. R Core Team (2022) R: A language and environment for statistical computing. (R Foundation for Statistical Computing, Vienna, Austria).
15. T. Hulsen, J. de Vlieg, W. Alkema, BioVenn - a web application for the comparison and visualization of biological lists using area-proportional Venn diagrams. *BMC Genomics* **9**, 488 (2008).
16. E. Ulgen, O. Ozisik, O. U. Sezerman, pathfindR: An R Package for Comprehensive Identification of Enriched Pathways in Omics Data Through Active Subnetworks. *Front Genet* **10**, 858 (2019).

Supplemental Figures and Figure Legends

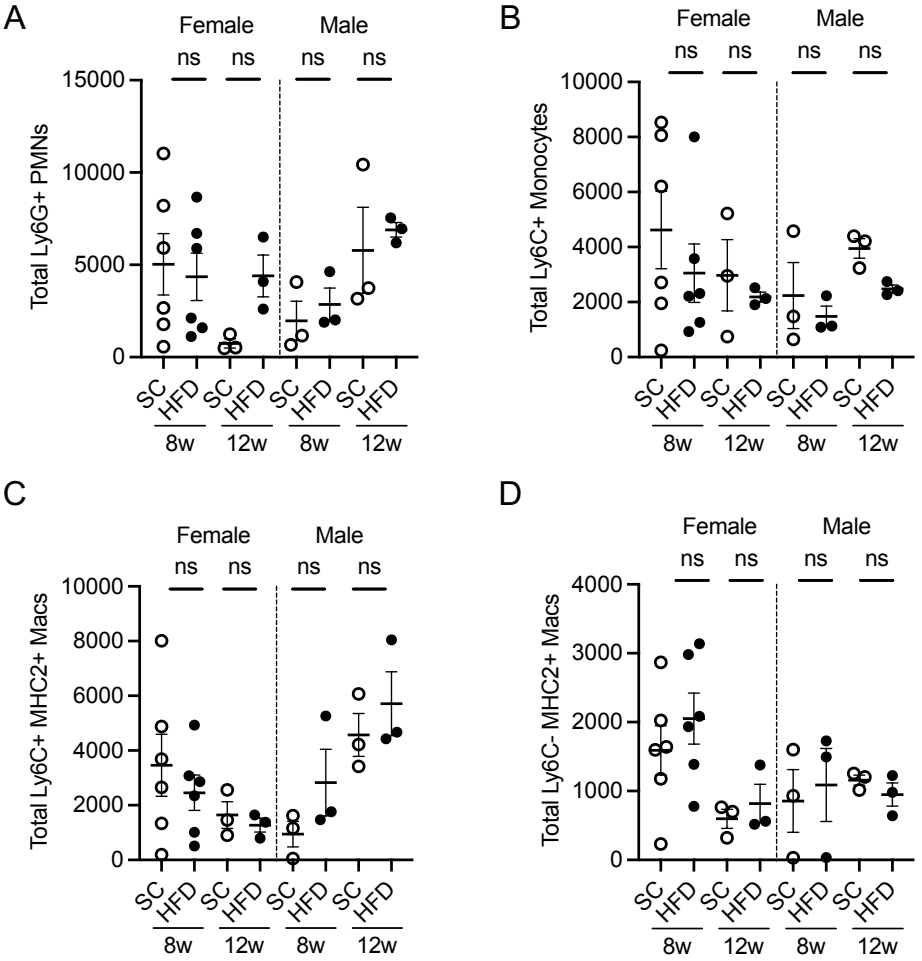

Supplemental Figure 1: Characterization of immune cell recruitment in UPEC-infected bladders. Female and male mice maintained on a HFD or SC were infected with UPEC and mouse bladders were collected for flow cytometry twenty-four hours after infection. (**A-D**) Plots of the absolute numbers of neutrophils (A), inflammatory monocytes (B), monocyte-derived macrophages (C), and resident macrophages (D) in infected bladders. Graphs show the mean and SEM. Each point denotes immune cell numbers in a unique mouse (*n*=3-6). Pairwise comparisons were performed between HFD and SC groups as indicated in graphs (Mann Whitney *U* test). **These data supplement Figures 1 and 2**.

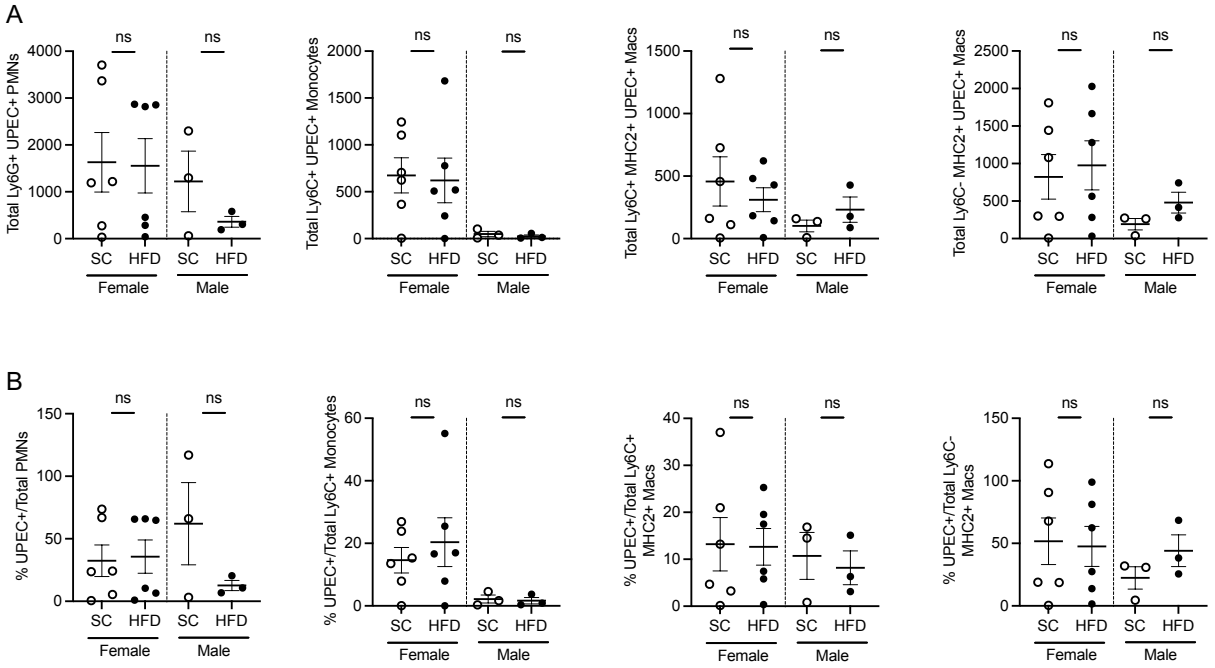

Supplemental Figure 2: Diet induced obesity does not impact UPEC phagocytosis. Female and male mice were maintained on a high-fat diet (HFD) or standard chow (SC) for 8 weeks, then infected with GFP-expressing UPEC. Bladders were collected twenty-four hours after infection for flow cytometry. (**A**) Plots of absolute numbers UPEC-positive neutrophils, monocytes, monocyte-derived macrophages, and resident macrophages, indicative of UPEC phagocytosis by these myeloid populations (**B**) Percent of UPEC+ cells within each immune cell population, reflecting the proportion of phagocytic activity. Graphs show the mean and SEM. Each point denotes immune cell numbers in a unique mouse (*n*=3-6). Pairwise comparisons were performed between HFD and SC groups as indicated in graphs (Mann Whitney *U* test). **These data supplement Figures 1 and 2.**

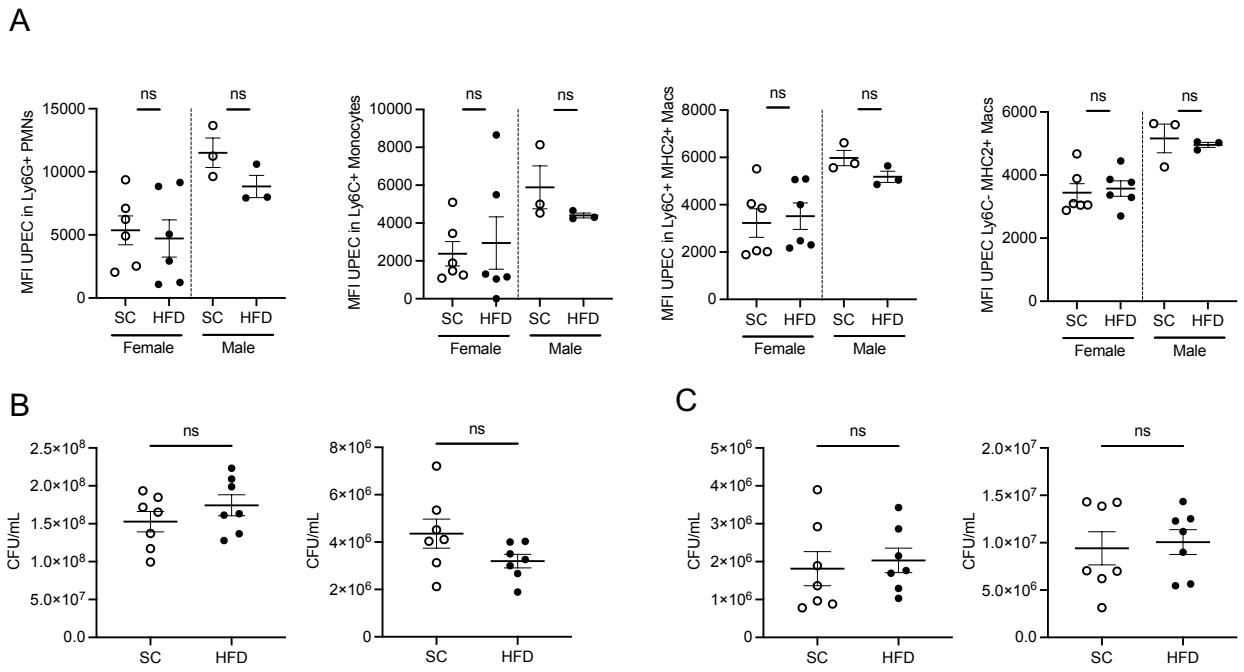

Supplemental Figure 3: Diet induced obesity does not impact intracellular or extracellular UPEC killing. (**A**) Female and male mice maintained on a high-fat diet (HFD) or standard chow (SC) for 8 weeks, then infected with GFP-expressing UPEC. Bladders were collected twenty-four hours after infection for flow cytometry. Plots illustrate mean fluorescence intensity (MFI) of GFP+ signal in neutrophils, monocytes, monocyte-derived macrophages, and tissue-resident macrophages. MFI serves as a surrogate to measure intracellular UPEC burden, with higher MFI reflecting increased UPEC survival or impaired killing. (**B**-**C**) Neutrophils were enriched from bone marrow of uninfected female mice maintained on a HFD or SC diet for 8 weeks, then challenged *ex vivo* with UPEC strain UTI89 (B) or CFT073 (C) at 100 MOI (left) or 1000 MOI (right). Following incubation, extracellular bacterial killing was enumerated and graphed as CFU/mL. Graphs show the mean and SEM. Each point denotes a direct measurement from an individual mouse (A) or neutrophils recovered from a unique mouse (B-C; *n*=3-7). Pairwise comparisons were performed between HFD and SC groups using the Mann Whitney *U* test. **These data supplement Figures 1 and 2.**

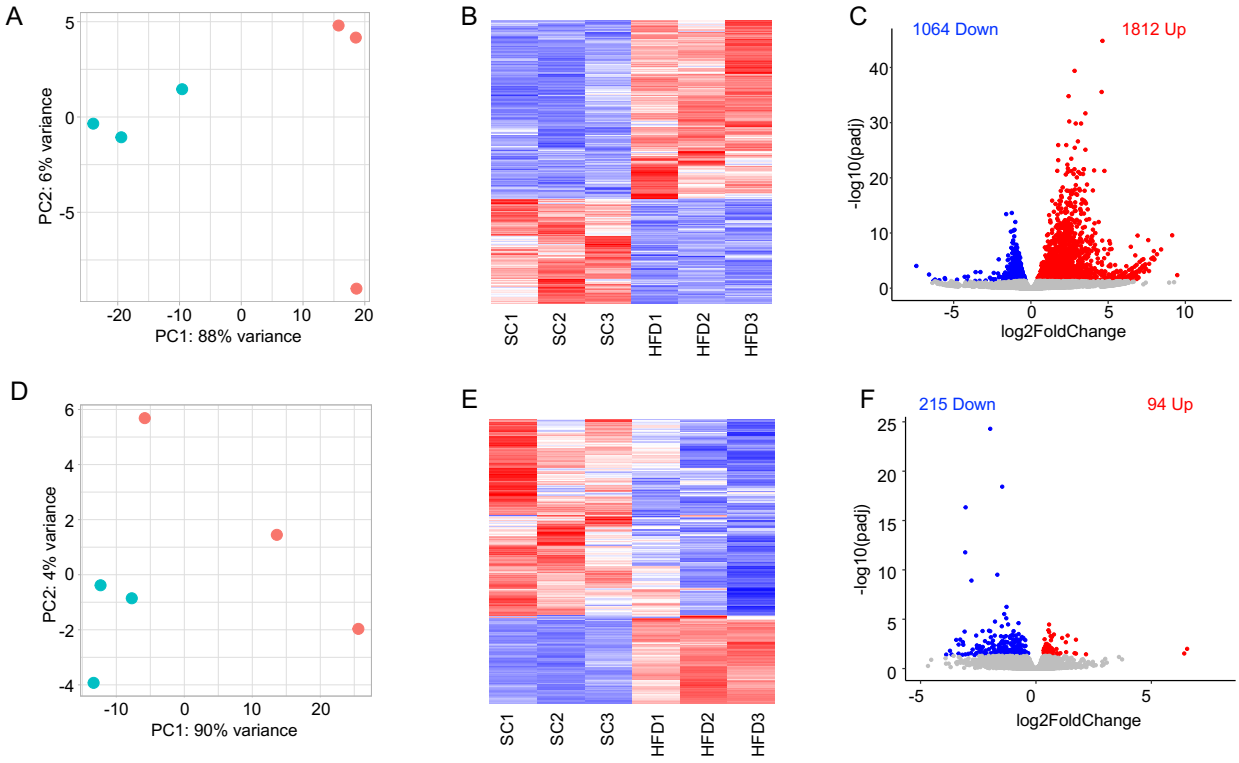

Supplemental Figure 4: Eight weeks of high-fat diet alters gene expression in the female and male urothelium. (**A/D**) Principal component analysis (PCA) plots from RNA-seq data of female (A) and male (D) urothelium after 8 weeks on standard chow (SC) or high-fat diet (HFD). Each symbol represents a urothelial sample from an individual mouse fed SC (green) or HFD (red). (**B**/**E**) Heatmaps showing differential gene expression between HFD and SC fed female (B) and male (E) urothelium, with each column representing an individual mouse. (**C**/**F**) Volcano plots illustrating differentially expressed genes expression between HFD and SC fed female (C) and male (F) urothelium. Red marks up-regulated genes with log2 fold change > 0 and adjusted *P*-value < 0.05. Blue marks down-regulated genes with log2 fold change < 0 and adjusted *P*-value < 0.05. Adjusted *P*-values were calculated using the Benjamini-Hochberg procedure.
These data supplement Figure 3.

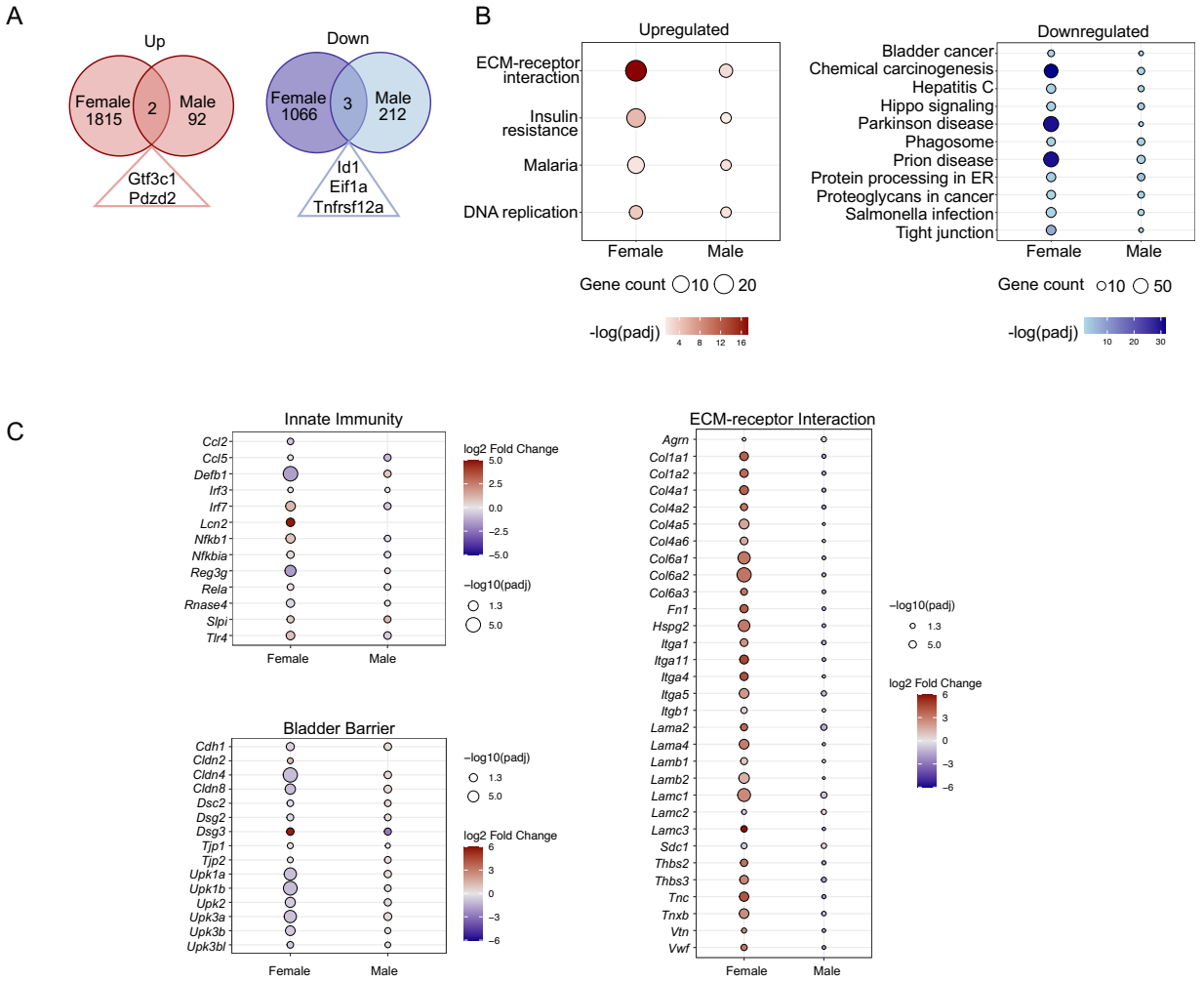

Supplemental Figure 5: Eight weeks of high-fat diet consumption leads to increased cell-ECM signaling in the urothelium. (**A**) Venn diagrams show minimal overlap between significantly up-regulated (left) and down-regulated (right) genes in female and male urothelium after 8 weeks on standard chow (SC) or high-fat diet (HFD). (**B**) KEGG pathway enrichment derived from up-regulated (left) and down-regulated (right) genes in HFD-fed female and male mice. Bubble size reflects the number of enriched genes per pathway and color indicates significance. (**C**) Expression of curated gene sets related to innate immunity, bladder barrier integrity, and ECM-receptor interaction. Bubble color represents log2 fold change (HFD vs. SC) and size indicates significance. (B-C) Significance was assessed via hypergeometric testing on active subnetworks identified from the protein-protein interaction network using PathfindR, with *P*-values adjusted using the Benjamini-Hochberg method. **These data supplement Figure 4**.

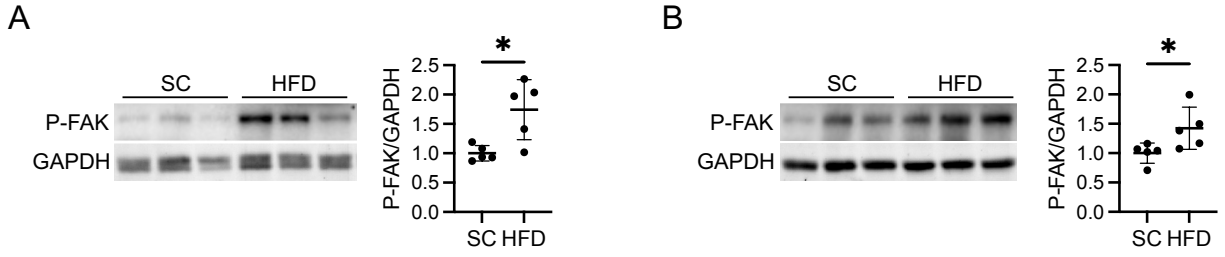

Supplemental Figure 6: Focal adhesion kinase signaling is elevated in total bladders during obesity. (**A/B**) Representative Western blots (left) and densitometry (right) of P-FAK (Y397) and GAPDH in total bladder lysates from female (A) and male (B) mice maintained on standard chow (SC) or high-fat diet (HFD) for 8 weeks. Quantification of Western blots was performed on bladders from 5 mice per group (n = 5). Graphs show the mean and standard deviation. Each point represents an individual mouse. Asterisks indicate significant P-values for the indicated pairwise comparisons (Mann-Whitney U test). *P < 0.05. **These data supplement Figure 5**.

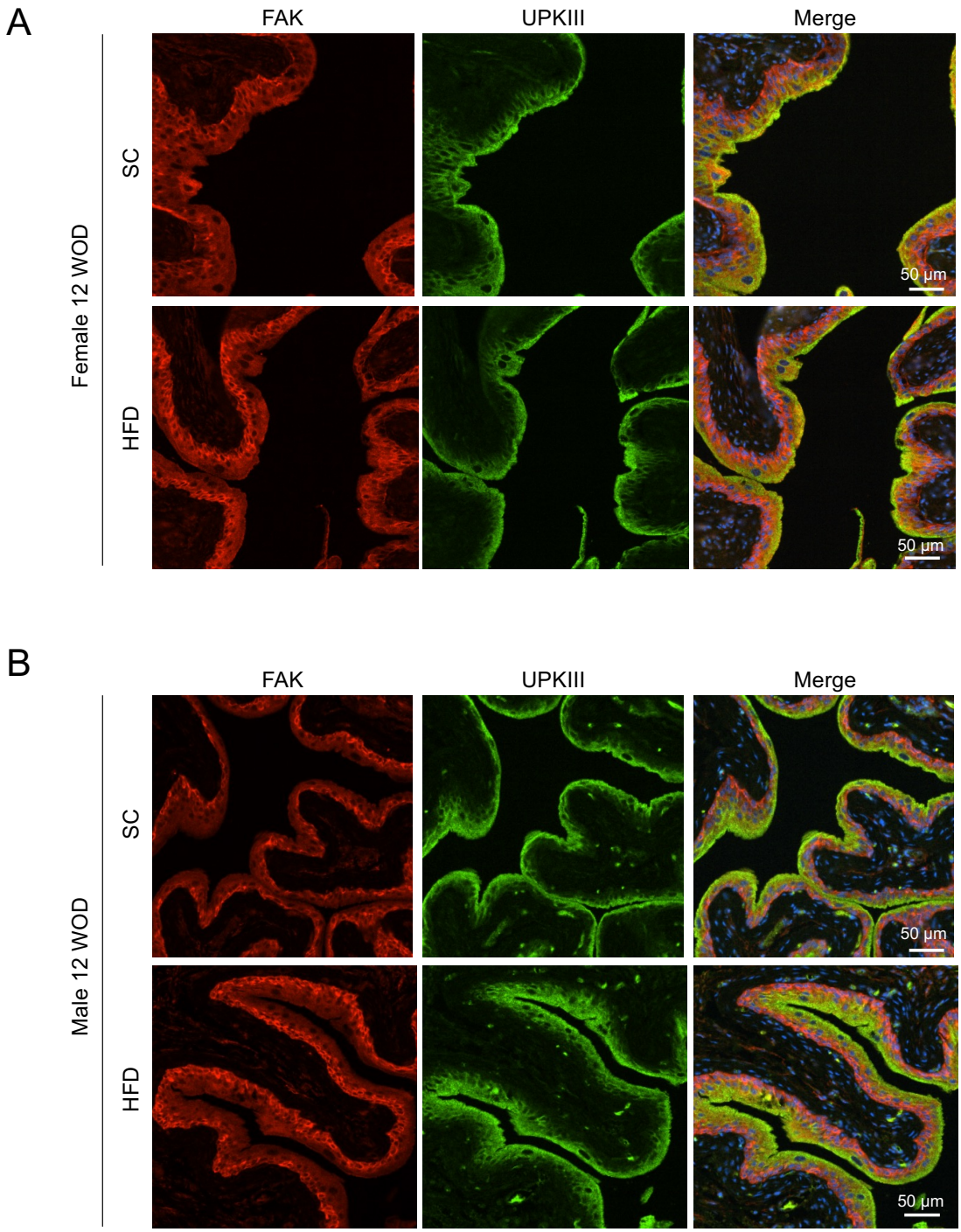

Supplemental Figure 7: Obesity increases urothelial FAK expression. Representative immunofluorescent bladder images from non-infected (A) female and (B) male mice after 12 weeks on standard chow (SC) or high-fat diet (HFD) labeled with antibodies to total FAK (red), uroplakin III (green) and nuclei (blue, Hoechst). Magnification = 20X. Staining was completed on 4 bladders per cohort. **These data supplement Figure 5**.

Supplemental Tables

	Female			Male		
	SC	**HFD**		**SC**	**HFD**	
Cytokine (pg/mL)	**Mean ± SEM**	**Mean ± SEM**	***P*-value**	**Mean ± SEM**	**Mean ± SEM**	***P*-value**
IFN-γ	22.05 ± 1.21	25.63 ± 1.28	0.073	30.62 ± 2.68	27.84 ± 4.58	0.277
IL-1β	< LOD	< LOD	NA	< LOD	< LOD	NA
IL-6	14.24 ± 0.35	15.89 ± 0.91	0.277	18.16 ± 1.17	19.42 ± 3.17	0.594
IL-10	69.58 ± 1.78	81.6 ± 3.04	**0.004**	81.6 ± 2.25	79.11 ± 3.94	0.435
IL-17A	40.5 ± 8.57	70.77 ± 12.87	0.073	102.3 ± 18.38	58.49 ± 12.51	0.128
TNFα	78.77 ± 10.07	96.34 ± 6.66	0.104	130.3 ± 20.69	94.32 ± 11.85	0.165

Supplemental Table 1: **Cytokine profiles in diet induced obesity male and female mice.** Serum cytokine profiles in female and male mice fed standard chow (SC) or a high-fat diet (HFD) for 12 weeks (*n* = 7 mice/cohort). *P*-values evaluate differences between sex-matched cohorts (Mann-Whitney *U* test). IL-1β was below the limits of detection.

Reagent	Vendor	Catalog Number
Mice		
B6.Cg-*Gt(ROSA)26Sor*$^{tm14(CAG\text{-}tdTomato)Hze}$/J	The Jackson Laboratory	Strain # 007914
Diet		
Teklad Chow	Inotiv	2920X
Standard Chow (SC)	Research Diets, Inc.	D12450Ji
High-Fat Diet (HFD)	Research Diets, Inc.	D12492i
Cell Culture		
Primary human urothelial cells (HBLAK)	CELLnTEC Advanced Cell Systems	HBLAK RRID:CVCL_JQ59
CnT-Prime Epithelial Proliferation Medium	CELLnTEC Advanced Cell Systems	CnT-PR
Phoenix-AMPHO cells	American Type Culture Collection (ATCC)	CRL-3213
Bacteria		
Uropathogenic *Escherichia coli* UTI89	Provided by Dr. Scott J. Hultgren	PMID: 2877947
Plasmids		
pWZL-Neo-Myr-Flag-DEST (empty)	Addgene	15300
pWZL-Neo-Myr-Flag-PTK2	Addgene	20610
pCMV-HA-PKBα-WT	Provided by Dr. Dario Alessi	PMID: 9395488
pCMV-HA- PKBα-M/P (membrane-targeted)	Provided by Dr. Dario Alessi	PMID: 9395488
Antibodies		
GAPDH	Cell Signaling Technology	2118
P-AKT (Ser473)	Cell Signaling Technology	4060
P-FAK (Tyr397)	Abcam	ab81298
M2-FLAG tag	Sigma Aldrich	F3165
HA Tag	Sigma Aldrich	05-904
FAK	Abcam	ab40794
Uroplakin IIIA	Fitzgerald	10R-U103ax
Goat anti-Rabbit (Cy3)	Jackson ImmunoResearch	111-165-003
Goat anti-Mouse (Alexa Fluor 488)	Jackson ImmunoResearch	115-545-003
Hoechst	Thermo-Fisher	PI62249
Brilliant Violet 785 anti-mouse CD45	BioLegend	103149, 30-F11
Alexa Fluor 700 anti-mouse/human CD11b	BioLegend	101222, M1/70
Brilliant Violet anti-mouse Ly-6C	BioLegend	128031, HK1.4
PerCP/Cy5.5 anti-mouse Ly-6G	BioLegend	127616, 1A8
Chemical Reagents		
DharmaFECT transfection reagent	Dharmacon	T-2001-02
Lipofectamine 2000	Thermo-Fisher	11668027
Halt Phosphatase and Protease Inhibitor	Thermo-Fisher	PI78445
Commercial Assays		
Nucleospin RNA Plus XS Kit	Takara Bio	740990
Clontech SMARTer v4 Ultra Low Input Kit	Takara Bio	634888
Nextera XT DNA Library Preparation Kit	Illumina	FC-131-1024
Bio-Plex Pro Mouse Cytokine Th17 Panel A	Bio-Rad	M6000007NY
Mojosort Mouse Neutrophil Isolation Kit	BioLegend	480058
siRNA Pools		
SMARTpool: Non-Targeting siRNA Pool	Horizon Discovery	D-001810-10-05
SMARTpool: ON-TARGETplus *PTK2* siRNA	Horizon Discovery	L-003164-00-0005

Supplemental Table 2: Key Reagents. List of mice, antibodies, chemical reagents, recombinant plasmids, and siRNA used with vendor and catalog number.

Dataset S1 (separate file): Differentially expressed genes in urothelium after 12 weeks of HFD vs SC diet feeding. These data supplement Figures 3 and 4.

Dataset S2 (separate file): Differentially expressed genes in urothelium after 8 weeks of HFD vs SC diet feeding. These data supplement Supplemental Figures 4 and 5.